Review

Envisioning Quantum Electrodynamic Frameworks Based on Bio-Photonic Cavities

Vincenzo Caligiuri [1,2], **Francesca Leone** [1], **Ferdinanda Annesi** [2], **Alfredo Pane** [2], **Roberto Bartolino** [2] **and Antonio De Luca** [1,2,*]

[1] Department of Physics, University of Calabria, Via P. Bucci, Cubo 31C, 87036 Rende, Italy; lnefnc94d69d086j@studenti.unical.it

[2] CNR-Nanotec Rende, Via P. Bucci, Cubo 31C, 87036 Rende, Italy; ferdinanda.annesi@cnr.it (F.A.); alfredo.pane@cnr.it (A.P.); roberto.bartolino@fis.unical.it (R.B.)

[*] Correspondence: vincenzo.caligiuri@unical.it (V.C.); antonio.deluca@unical.it (A.D.L.)

Abstract: A bio-photonic cavity quantum electrodynamic (C-QED) framework could be imagined as a system in which both the "cavity" and the "atom" participating in the light-matter interaction scenario are bio-inspired. Can a cavity be made of a bio-polymer? If so, how should such a cavity appear and what are the best polymers to fabricate it? Can a bioluminescent material stand the comparison with new-fashion semiconductors? In this review we answer these fundamental questions to pave the way toward an eco-friendly paradigm, in which the ever-increasing demand for more performing quantum photonics technologies meets the ever-increasing yet silent demand of our planet to reduce our environmental footprint.

Keywords: bio-photonic cavities; quantum electrodynamic framework; light matter interaction; bio-photonics; bio-materials; biodegradable photonics; biodegradable metamaterials; bio-inspired metamaterials; fluorescent proteins

1. Introduction

The interaction between light and matter is the process due to which an electromagnetic radiation releases energy to matter by interacting with its molecular or atomic structure. Light-matter interaction processes are countless and involve all the dynamics that, for example, sustained life development on Earth. Chlorophyllian photosynthesis constitutes, perhaps, the most elegant example of light–matter interaction. The core of such reaction is chlorophyll, a molecule capable of selectively absorbing sun radiation and converting it into an internal charge separation via the excitation of the molecule from the ground state to an excited one. Such a coherent charge delocalization in a light-absorbing molecule is often called an *exciton*, and represents the quantum of the electronic excitation in a solid [1–3]. Excitons are therefore the first actors playing on the light–matter interaction stage.

A penetrant intuition from Albert Einstein elucidated that the light–matter interaction occurs on a discrete scale rather than a continuous one, fostering the hypothesis to associate the color of light to the energy carried by the photon [4]. For this reason, light–matter interaction processes are better (but not only) described in the framework of quantum mechanics, where an already appropriate formalism to describe a discrete world is common [5].

Once excited in a photoluminescent molecule, excitons can radiatively relax by emitting a photon with approximately the same energy of the exciton. If the molecule is placed in proximity of a resonant cavity, these two elements can interact "weakly" or "strongly". Classic optics describes a resonant cavity as constituted by two highly reflecting mirrors facing each other and displaced by a distance D, determining the discrete set of allowed resonances (modes) of the cavity (Figure 1a). Such a configuration is sometimes called a

Fabry–Pérot resonator, the optical cavity by antonomasia [6,7]. In a Fabry–Pérot, therefore, given a certain value of *D*, the entrapment and propagation of only precise wavelengths can be sustained. It is however true that the concept of a resonant cavity can be stretched and extended to resonant architectures shaped in unconventional ways that could be very distant from the two-facing-mirrors cliché.
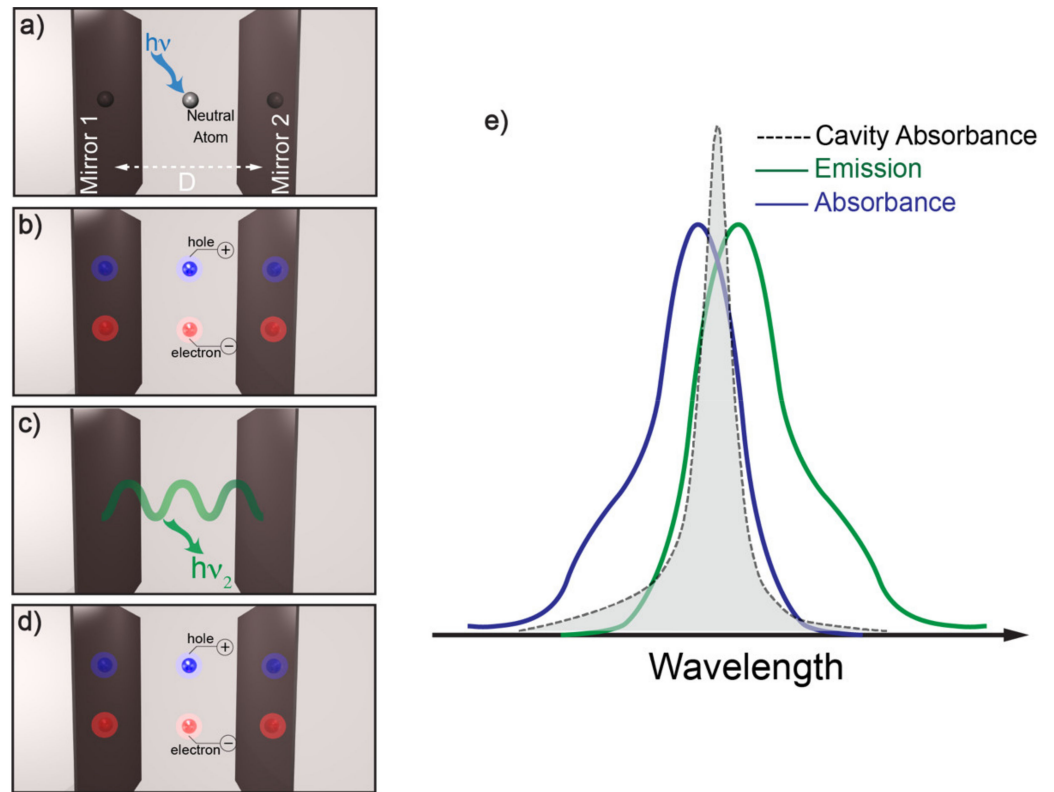

Figure 1. Sketch of the feedback mechanism at the basis of cavity–atom strong interaction. (**a**) Atom or molecule in its ground state placed between a classic Fabry–Perot cavity made of two mirrors facing each other, displaced by a distance D. If a photon with energy *hv* suitable to promote the atom or the molecule to an excited state interacts with the atom or molecule, an exciton is formed (**b**). The exciton can radiatively relax by emitting a photon with energy hv_2 very close to that of the exciton. The exciton can be stored in the cavity for many roundtrips (according to the Q-factor of the cavity) as a standing wave (**c**). Provided a low-Stokes-shift molecule, the photon stored in the cavity can be re-absorbed by the molecule and excite another exciton (**d**). (**e**) A proposed spectral configuration to optimize the cavity–atom interaction. Here, the cavity absorbance spectrum is designed to cover the spectral region in which the absorbance and the emission of the gain molecule overlap.

A weak cavity–atom interaction is usually accomplished by simply placing the atom or molecule (the physical entity embodying the concept of "matter" throughout this review) in the proximity of the cavity. The simple presence of an adequately tuned resonant system (the cavity) in its proximity, offers an additional relaxation channel to the exciton generated in an emitter (atom or molecule) brought to an excited state. The additional energy dissipation channel offered by the cavity can significantly modify the photophysics of the spontaneous emission processes of the emitter, especially through an effect known as the "Purcell effect" [8–13]. According to what was found by Purcell himself, if a quantum system is brought to interact with a resonant cavity, its spontaneous emission probability can be enhanced by a factor $f = 3Q\lambda^3/(4\pi^2 V)$ [14]. Here, Q is the quality factor of the resonant cavity (Q = $\lambda_0/\Delta\lambda$, λ_0 being the central wavelength of the cavity and $\Delta\lambda$ the full-width-at-half-maximum), $\lambda = \lambda_{free}/n$ is the wavelength assumed by the radiation, with a free-space wavelength equal to λ_{free}, within a cavity made of a material of refractive

index n placed between the two reflecting mirrors. V is a quantity called "modal volume", that was at first roughly expressed as the volume of the resonator, but whose definition has been subsequently refined and generalized [15–17]. The calculation of the correct modal volume for a particular structure can be a delicate task to accomplish [18]. However, some noticeable examples have been provided for the most widely used architectures: (i) photonic crystals (see Equation (1)) [19], (ii) nanocube antennae (Equation (2)) [20], (iii) dielectric pillar nanocavity and metal/dielectric cavities (Equation (3)) [21,22]:

$$V_{eff} = \frac{\int_V d^3r \left(\varepsilon(r) \left| \vec{E}(\vec{r}) \right|^2 \right)}{\varepsilon(\vec{r}_{max}) \max\left[\left| \vec{E}(\vec{r}) \right| \right]^2} \left(\frac{2n(\vec{r}_{max})}{\lambda} \right)^3 \tag{1}$$

where $\vec{r}_{max}$ is the position of the maximum of the squared electric field, ε and n are, respectively, the dielectric permittivity and the refractive index of the material in which the electric field **E** is confined and λ is the wavelength in the resonator.

$$V_{eff} = \frac{\int_V d^3r \left(\varepsilon(r) \left| \vec{E}(\vec{r}) \right|^2 \right)}{\max\left[\left| \varepsilon(r) \vec{E}(\vec{r}) \right| \right]^2} \tag{2}$$

$$V_{eff} = \frac{\int_V d^3r \left(\varepsilon(r) \left| \vec{E}(\vec{r}) \right|^2 \right)}{n_{bulk}^2} \tag{3}$$

where n_{bulk} is the refractive index of the bulk material taken as a reference.

The peculiarity of the weak interaction regime is that the two interacting systems keep on holding their original nature, so that the observer always deals with a pure exciton and a pure cavity mode.

The cavity–atom interaction regime can change dramatically, however, if a certain amount of feedback is introduced between the cavity and the gain material. For example, let us consider the case in which an emitter in its ground state is embedded in a resonant cavity (Figure 1a). Upon absorption of a photon carrying an appropriate energy, an exciton can be generated (Figure 1b). The exciton can then radiatively recombine by emitting a photon (Figure 1c). If the energy of the emitted photon is very close to that of the exciton (this is the case of dyes with a very low Stokes' shift) and the cavity is tuned to resonate at the energy of the exciton, the photon can be stored inside the resonant cavity for a certain number of roundtrips (Figure 1c) in the form of a standing wave. This process causes the available photon to be re-absorbed by the molecule and, therefore, to excite another exciton. Such a feedback mechanism lays the basis for what is called "strong light-matter interaction" [2,3,23–30]. A wise way to engineer a cavity–atom system envisioning the optimization of their strong interaction is the one illustrated in Figure 1e. By providing a low-Stokes-shift emitter (namely a photoluminescent material in which a significant portion of the absorbance and emission spectra overlap), the cavity should be tuned in such a way that its spectrum (the set of wavelengths that can be stored within it, which corresponds to the gray part of Figure 1e) covers the largest part of the spectral region in which the emission and absorption bands of the gain material overlap.

It goes without saying that the second actor on the light–matter interaction stage is the resonant cavity.

Maximizing the feedback mechanism occurring between the cavity and the exciton is a fine art. Such a task could be accomplished from a duplex point of view: (i) by optimizing the properties of the photoluminescent material, and (ii) by optimizing the properties of the resonant cavity. The photoluminescent material and the cavity can, therefore, be

considered the two ingredients constituting the "quantum framework" in which the light–matter interaction takes place. Their fundamental properties determine the capability of a system to access light–matter interaction regimes that are still unexplored. Both the gain material and the cavity are responsible for the environmental harmfulness of the quantum framework and, as will be shown hereafter, an eco-friendly approach is often sacrificed to achieve better performances. The difficulties in adopting an eco-friendly approach are numerous, hidden in both sides of the photoluminescent material and the cavity. Facing them requires a total paradigm shift. If, indeed, materials commonly employed in classic photonics have to be replaced with an eco-friendly counterpart, like a biopolymer, then classic architectures like Fabry–Pérot cavities also have to be ruled out from the design possibilities.

To meet the philosophy espoused by such a review implies, therefore, three main steps: (i) to identify planar resonant structures capable of providing an exceptional Q-factor resonance opening, at the same time, to allow for the possibility of a replica-molding in a biopolymer, (ii) to identify the ideal biopolymer to carry out the replica-molding process, and (iii) the most performing bioluminescent molecule to serve as an exciton reservoir. Therefore, this review is focused on illustrating all those readily available technological solutions to address the aforementioned steps, envisioning the structuring of a totally eco-friendly and bio-inspired quantum framework for light–matter interaction. For this reason, the review is structured as follows: Section 2 is dedicated to the description of the most promising and novel planar architectures belonging to the family of meta-Surfaces, which manifest a high-Q-factor resonant behavior. In Section 3 we provide some remarkable examples of biopolymers that could be ideal to replicate the architectures described in Section 2 via soft-lithography, whereas in Section 4 we browse some of the most performing bioluminescent materials that could be employed as the active core of the proposed paradigm. The broad and long-term vision of this work aims to lay the basis to bridge the worlds of meta-surfaces, biopolymers and bioluminescent molecules, in order to produce a new generation of bio-inspired, eco-friendly and nano-photonically engineered quantum framework, in which to tailor deeper and still unexplored light–matter interaction scenarios.

2. Resonant Meta-Surfaces

As mentioned in the introduction, the first step toward the design of a bio-inspired cavity quantum electrodynamics framework is to select the right resonator. If a bio-inspired approach has to be followed, from which commonly used materials for optoelectronics are excluded, then the puzzle raises its intricacy. In this case, indeed, due to the inability of common bio-inspired and biodegradable materials to behave like metals or dielectric mirrors, commonly used optoelectronic architectures are ruled out. New paradigms have to be explored, such as the so-called resonant meta-surfaces [31–33].

Meta-surfaces are novel nano-architectures whose performance and miniaturization capabilities are challenging the certainties of classic optics [34]. The prefix "meta" refers to meta-materials, the wider category to which meta-surfaces belong, since their properties go well beyond those of the constituent materials, and are mainly determined by their geometry. The term "surface", instead, points out that these structures share a planar nature which is in perfect agreement with the use of biopolymers. In other words, meta-surfaces (MS) can be considered as nanostructured surfaces whose optical response can be engineered at will to accomplish a particular optical task. To achieve a specific functionality, meta-surfaces can rely on both metallic or dielectric nano-elements [35–44]. For our purposes, dielectric meta-surfaces are the ones of interest. Manifesting high-Q resonances in the visible range is only one of the results achievable with meta-surfaces [45–62].

One way to achieve a high-Q-resonant response by means of a meta-surface is to engineer a so-called "biperiodic" disk lattice [62]. Such a recently studied configuration relies on a particular lattice arrangement of high-refractive-index dielectric elements in which the unitary cell consists of two disks: a larger one, with a diameter equal to $d + (\Delta/2)$,

and a smaller one, with a diameter of $d - (\Delta/2)$ (see Figure 2a). In the case reported in ref. [35] d = 92 nm, Δ is a spatial component to be added to d to obtain the large disk and to be subtracted to d to obtain the small disk. The asymmetry of the system can be evaluated via an "asymmetry parameter" $\alpha = \Delta/d$. In the case in which $\Delta = 0$ nm ($\alpha = 0$), corresponding to the mono-periodic lattice, no high-Q resonances are present in the transmittance spectrum (see Figure 2b, dashed line). When a small asymmetry is introduced between the two disks composing the unitary cell, such that Δ = 9.2 nm ($\alpha = 0.1$), two steep minima in the transmittance spectrum arise, constituting the high-Q-factor resonances excited in the bi-periodic meta-surface. These resonances are found to possess a dipole-like character. In particular, the high-wavelength resonance has a magnetic-like character (m_α), while the other has an electric-like character (p_α). The Q-factor of these modes is about 500 and 1000, respectively, but it can be further increased by changing the asymmetry of the unitary cell.
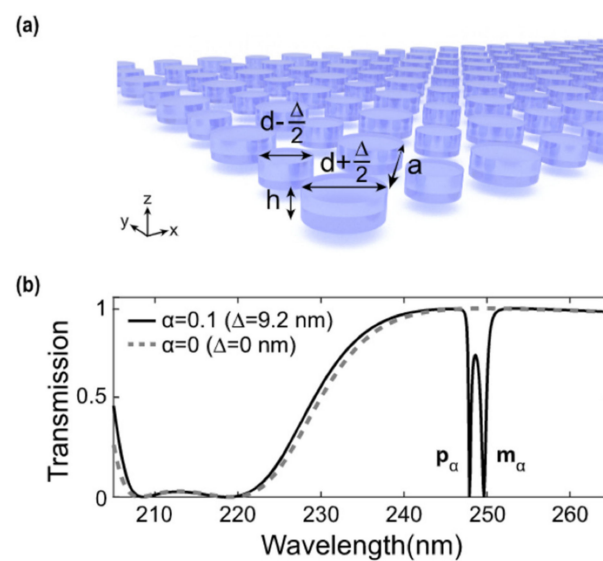

Figure 2. Biperiodic meta-surfaces: (**a**) Sketch of a biperiodic meta-surface made of a larger element with a diameter equal to d + ($\Delta/2$) and a smaller one of diameter d-($\Delta/2$). (**b**) Transmittance spectra belonging to two different cases. The first one, in which Δ = 0 (no biperiodicity), and the second one, in which Δ = 9.2 nm. In this latter case, two steep minima in the transmission spectrum of the structure are found, corresponding to the high-Q-factor resonances. Reproduced with permission from reference [62]. Copyright 2020, American Chemical Society.

Another remarkable example of high-Q-factor meta-surfaces are those in which the insurgence of resonances is governed by the so-called "Bound states In the Continuum" (BIC) [53–55,58–61,63–68]. BICs are common phenomena in many fields of physics, such as optics and acoustics. Let us consider, for example, the simple and general case of a wave propagating in the harmonic regime $e^{-i\omega t}$. We also consider a certain generic potential which sustains a set of discrete bound states (see Figure 3). The discrete set of bound states sustained by the potential are the familiar cases of the bound states of an electron in an atom or the modes of a metal/insulator/metal cavity or those sustained by an optical fiber. Outside the "discrete" set, a set of modes exists in the "continuum" as scattered waves. In addition, locally confined waves with a complex frequency $\omega = \omega_a - i\gamma$, ω_a being the resonant frequency, can arise in the continuum coupled with propagating waves. These waves assume the shape of "leaky resonances". Apart from these three cases, non-leaky bound states can exist in the continuum. These modes are known as "bound states in the continuum". BICs can be considered as the ideal ($\gamma = 0$) case of a leaky resonance with no losses and an infinite quality factor. It is however true that such a wave would be characterized by a completely non-radiative nature, being by definition decoupled from a radiative leaky wave. As such, it would be impossible to excite BICs with free-space

light. In practice, only low-loss BICs or "quasi-BIC" modes can be excited via free-space light illumination. The concept of a bound state in the continuum has been originally introduced in the field of quantum mechanics by Von Neumann and Wigner [69]. However, Fredrich and Wintgen generalized it in terms of a destructive interference between two resonances which would originally be decoupled, but that, as a consequence of the tuning of a particular parameter, can be brought to interact and strongly couple with each other [70].
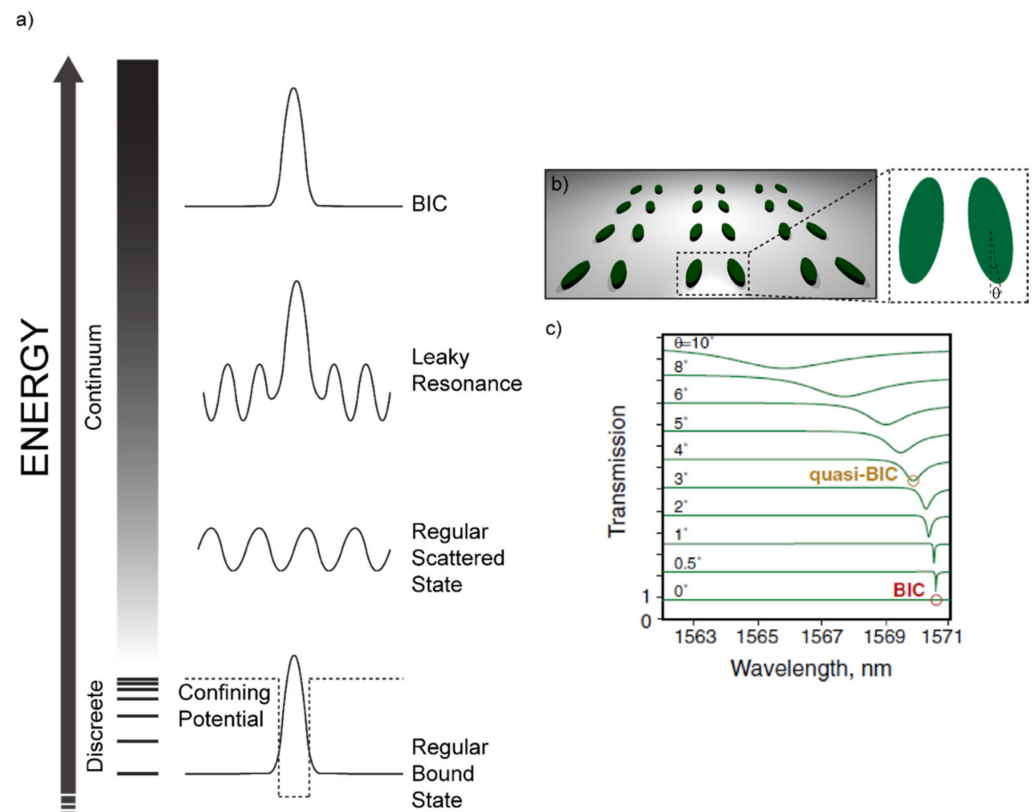

Figure 3. Bound States in the Continuum: (**a**) Sketch of the possible states in the "discrete" and in the "continuum" sets. If a potential is structured in such a way that only a discrete set of modes is allowed, then regular bound states will appear due to the confinement action of the potential itself. If the energy is higher than the height of the potential barrier, a continuum of allowed states is accessed. The simplest and most probable state in the continuum is a regular scattered state. A so-called "leaky resonance" can occur in the continuum due to some kind of destructive interference phenomenon that suppresses some of the radiative channels and forms a bound state. Such a leaky bound state or leaky resonance is also coupled to a scattered (radiative) wave and, therefore, can be accessed by free-space light. In the end, a Bound State in the Continuum (BIC) can occur if the aforementioned mechanism for the leaky resonances suppresses all the radiative channels, thus forming an ideal bound state in the continuum. The illustration is inspired by reference [71]. (**b**) Sketch of the architecture re-drawn from references [60,72], evidencing the tilt angle θ as the tuning parameter to access the quasi-BIC visible as steep minima in the transmittance spectrum shown in (**c**). Reproduced from reference [60].

If the parameter that enables the coupling between these two modes intervenes on the symmetry of the system, we are in presence of a "symmetry-protected BIC". These BICs are of special interest for the purpose of this review, since they occur in structures that can be readily replicated with a biopolymer through a soft-molding technique. Indeed, when a particular system holds a degree of symmetry (a reflection or rotational symmetry, for example), the modes with different symmetry classes are totally decoupled. However, if the symmetry is somehow broken, these modes can be brought to interact [71]. One noticeable example belonging to this family of symmetry-protected BICs consists in a lattice made of a zigzag array of tilted silicon resonators, as shown in Figure 3b [71]. The tuning parameter

here is the tilt angle θ of the long axis of one of the facing elements. At $\theta = 0°$, such a structure is found to have a symmetry-protected BIC that is impossible to excite through free-space light. However, while tilting θ, the symmetry is broken, and quasi-BIC modes become accessible. Such modes appear as steep minima in the transmission spectrum, whose Q-factor decreases while increasing θ and, as a consequence, departing from the perfect symmetry condition.

3. Biopolymers for Soft-Molding Processes

As mentioned earlier, the adoption of a planar resonant structure is paramount to envision a bio-inspired photonic architecture employing biopolymers as the material of choice. Polymers like Polydimethylsiloxane (PDMS) can, indeed, be usually structured at the micro- and nano-scale via a technique called replica molding [73]. Through this process, any kind of nano-structure can be impressed over the polymer surface by simply pouring the polymeric liquid solution over a solid master, engineered with the "negative" shape [74–78].

Replica molding processes are usually carried out with soft elastomers like PDMS, which can be considered as a standard for these processes. Among all other properties, PDMS is also bio-compatible. Unfortunately, it is not biodegradable. Since the leitmotif of this review is to look for a reduction of the environmental footprint left by nano-technology, bio-inspired polymers are going to be targeted, keeping PDMS as a benchmark to be overcome. Natural biopolymers stand out for many aspects, including their light weight, excellent mechanical properties, biocompatibility, non-toxicity, low cost, etc. Thanks to these superior merits, natural functional biopolymers can be designed and optimized for the development of high-performance bio-photonic components [79]. Before describing in detail some of the most interesting technologically mature solutions, we list hereafter (Table 1) some of the many characteristics that make biopolymers the ideal choice as a bio-compatible scaffold with respect to classic soft elastomers [80–82]:

Table 1. Comparison between the proposed biopolymers with respect to PDMS.

Polymer Property	Silk	Cellulose	Hydrogel	PDMS
Mechanical property	Excellent	Good	Good	Good
Optical clarity	Excellent	Excellent	Very Good	Moderate/Negative
Biocompatibility	Excellent	Excellent	Excellent	Good
Biodegradability	Excellent	Excellent	Excellent	Negative
Low absorption	Excellent	Excellent	Moderate	Negative
Tunable fluorescence			Moderate	Negative
Rapid prototyping	Moderate	Moderate	Moderate	Negative

3.1. Silk

A special place in the family of bio-inspired polymers for optics is occupied by silk fibroin. Silk can be easily extracted from the cocoons of *Bombyx mori* Lepidoptera through a multistep procedure involving (i) silk cocoon degumming through a boiling process, (ii) dissolution in a salt solution and (iii) transformation in an aqueous solution via dialysis [83] (see Figure 4).
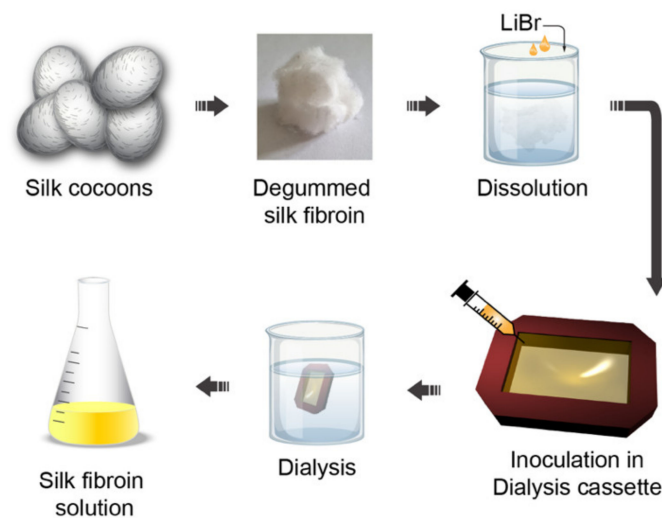
Figure 4. Silk fibroin water solution fabrication: Silk cocoons are degummed through a boiling process and dissolved in a LiBr salt solution. The obtained solution is inoculated in a dialysis cassette and dialyzed for 48 h in ultrapure water. After that, the dialyzed solution is stirred to obtain the silk fibroin in aqueous solution. Inspired by references [83,84].

Once silk fibroin is obtained in an aqueous solution, it is readily available for the most variegated nano-engineering processes. Replica molding for microfluidic structures has probably been the first application on which micro-structured silk fibroin devices have been based [85–87].

For example, 3D silk photonic crystals have recently been obtained in the form of a three-dimensional inverse opal [61] (see Figure 5). The fabrication technique is easy yet effective. A 3D opal of polystyrene PS beads is obtained through a bottom-up technique, and then the aqueous silk fibroin solution is infiltrated in the opal and left to dry. In the end, the composite is immersed in toluene to dissolve the PS beads and obtain a silk inverse opal. Such a structure can be tuned via UV light exposure, which can also be easily localized by using proper shadow masks, or water vapor (WV) exposition.
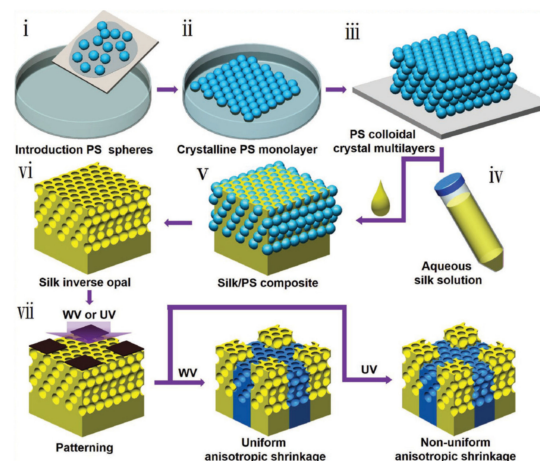

Figure 5. Three-Dimensional silk photonic crystal: (**i**) PS beads are deposited over the water surface via a hydrophilic substrate. (**ii**) The sphere forms a crystalline monolayer at the water/air interface through self-assembly. (**iii**) Colloidal crystals are generated by subsequent scooping transfer procedures from the water/air interface to the sphere-coated substrate. (**iv**) The aqueous silk solution prepared as mentioned before is (**v**) introduced in the so-formed PS sphere 3D photonic crystal. (**vi**) The silk 3D inverse opal is obtained by dissolving the polystyrene beads in toluene. (**vii**) The silk inverse opal is shadow-masked and exposed to WV (water vapor) or UV light to obtain the desired pattern. Reproduced with permission from reference [88].

Such a mechanism can be further refined to use the silk inverse opal as a canvas for nano-scale resolution painting. The chemical "brush" consists of a cartridge loaded with a methanol–water (MeOH) mixture capable of inducing local conformational changes in the silk inverse opal, and thus locally changing its lattice constant. Such a fascinating technique can be understood as a form of humidity photonic structural painting [89].

The silk fibroin has also proved valuable as an all-water based Electron Beam (E-beam) resist, both positive and negative [90]. The two concurrent mechanisms that allow silk fibroin to behave as a positive (wash away the exposed area) or negative (wash away the non-exposed area) resist are (i) the formation of water-soluble peptides (in the case of the positive resist) and (ii) water radiolysis (for the negative case). In the former case, silk fibroin in an aqueous solution is crystallized to manifest water-insoluble properties. Under electron beam irradiation, the proteins composing such silk crystals degrade due to inelastic collisions with electrons. This process produces water-soluble peptides that can be easily washed away with water. In the latter case, water radiolysis, occurring as a consequence of high electron beam doses, induces a helicoidal folding of silk fibroin with the formation of intermolecular crosslinks that make the exposed area water-insoluble. The possibility to dope the silk fibroin's aqueous solution with dyes like Green Fluorescent Protein (GFP), quantum dots and enzymes has been investigated with success, producing photoluminescent and bio-compatible E-beam resists.

3.2. Cellulose

An exceptional alternative to non-biodegradable polymers for replica molding applications is represented by cellulose. Cellulose consists of a chain of D-glucose units linked via a glycosidic bond, a particular kind of covalent bond that links the OH group of a sugar molecule to an atom or another molecule. In the case of cellulose, the glycosidic bond occurs between the OH group present on the C_1 of the first monosaccharide and the C_4 of the subsequent monosaccharide, by eliminating one water molecule to form a long polymeric chain. Hence, cellulose can be considered as the "polysaccharide" skeleton of a large part of the vegetable reign [91].

Its large availability (an annual world biomass production of about 10^{12} tons), united with consolidated extraction and purification procedures, makes cellulose one of the most known and technologically explored biopolymers. Highly demanded features such as hydrophilicity, water insolubility, chirality, biodegradability and broad chemical functionalization capability are naturally possessed by cellulose, making it an inexhaustible framework in which to develop a variegated plethora of technologies. Actually, cellulose played a pivotal role in spreading written culture and developing human thinking, considering its use since ancient Egypt as a technological material for the production of papyri. The textile industry, on its side, fostered a deep knowledge of cellulose chemistry to produce increasingly efficient filaments, like "viscose" [92]. There are mostly four pathways for the production of cellulose: (i) extraction from plants, (ii) bio-synthesis from bacteria, fungi and algae, (iii) in vitro cellulose synthesis and (iv) chemosynthesis by ring-opening polymerization. The first one is by far one of the most used. Relatively pure cellulose fibers can be extracted from cotton. However, if agro-wastes from, for example, cocoa, tomato pomace, and similar sources [93] have to be used within a circular economy framework, then purification techniques are mandatory. In these cases, a multistep procedure can be followed. As a first step, the vegetables from which cellulose must be extracted are dried in an oven overnight to remove water as well as other sugars and alcohol residuals. Then, the dried materials are dispersed in trifluoroacetic acid (TFA). The last step consists of centrifuging the solutions, so that the remaining clear solution can be easily cast over the desired substrate. In Figure 6, such a multistep procedure is illustrated together with films produced from cocoa pod husks, rice husks, parsley stem and spinach stem.
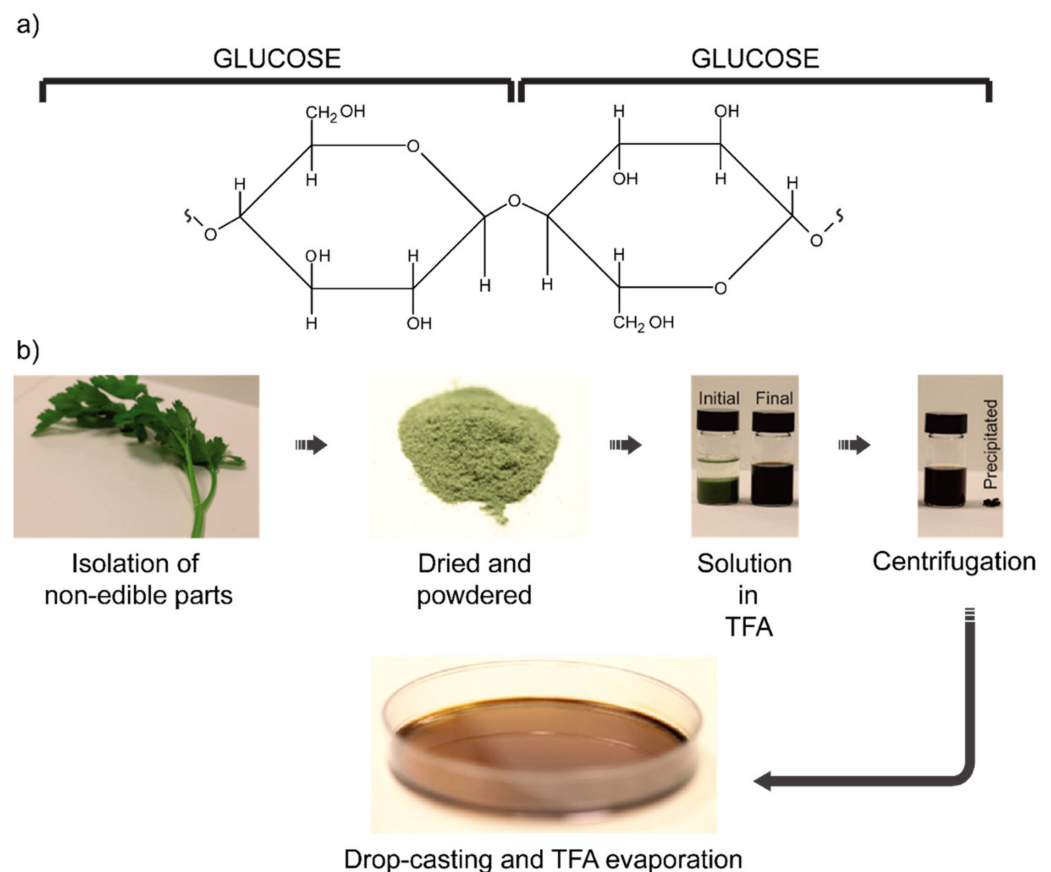
Figure 6. Cellulose structure and preparation: (**a**) Cellulose polymeric chain formed via glycosidic bond between multiple D-glucose subunits. (**b**) Cellulose purification scheme for the achievement of bioplastics from non-edible agro-wastes. Powdered wastes from vegetables are dissolved in TFA, centrifuged and casted to let the solvent evaporate and obtain the film. Reproduced with permission from reference [93], Copyright 2014, American Chemical Society.

The obtained purified cellulose solution can be directly used to replicate micro- and nano-structures for high-end photonics. For example, purified cellulose has been recently used as a biodegradable and water-insoluble scaffold for the molding of photonic crystals and meta-surfaces in applications as optical diffraction gratings, structural dielectric colors, plasmonic resonators and Surface-Enhanced Raman Scattering (SERS) [94] (see Figure 7).

If additional water solubility is demanded, hydroxypropyl cellulose (HPC) can be used instead of the pure version [95]. HPC is a water-soluble substance derived from cellulose to which hydroxypropyl groups are added—a feature that, among the other chemical modifications, carries additional OH groups, which make HPC even more reactive than pure cellulose. HPC-based sub-micrometric structures have been produced via both hot embossing and replica-molding techniques, showing exceptional optical and plasmonic properties [95].

Moreover, cellulose nanocrystals (CNCs) can also display cholesteric liquid crystalline phases. Cholesteric liquid crystals (CLCs) are chiral mesostructures whose pitch induces a Bragg-like reflection band which can be easily understood as the photonic band-gap of 1D photonic crystals [96–101]. Considering the disruptive impact CLCs had in tunable and active optics, micro-lasers and other devices, it is easy to figure out the potentialities of the cholesteric phases of crystalline cellulose [102]. CNCs are obtained, in general, via acid hydrolysis [103–107]. The choice of the acid for the hydrolysis process is determinant in the stability of the produced colloidal CNCs suspensions. The best results have been obtained by using H_2SO_4, since such a process introduces sulfate half-ester groups into the CNC surface, a feature that improves the colloidal stability of the produced CNCs in

water [108–110]. Once CNCs are obtained, chiral nematic phases are gradually approached while increasing the concentration of CNCs in a water solution [111,112]. In highly diluted suspensions, CNCs distribute themselves in an isotropic phase. While increasing the concentration above a critical threshold, chiral nematic phases appear in the form of localized liquid crystalline droplets called "tactoids" [113–116]. The pitch of the cholesteric phase of the polymer is even influenced by the source from which CNCs are extracted [103]. Cellulose extracted from wood pulp, for example, is suitable to obtain pitches of about 100–300 nm, while those extracted from bacteria, tunicates and cotton lead to pitch lengths of around 500–2000 nm, 1000 nm and 100–400 nm, respectively [97,108,117]. Cholesteric phases in CNCs have been recently analyzed via hyperspectral imaging, a tool that provides incomparable investigation possibilities regarding the defect structures in CNCs [118].
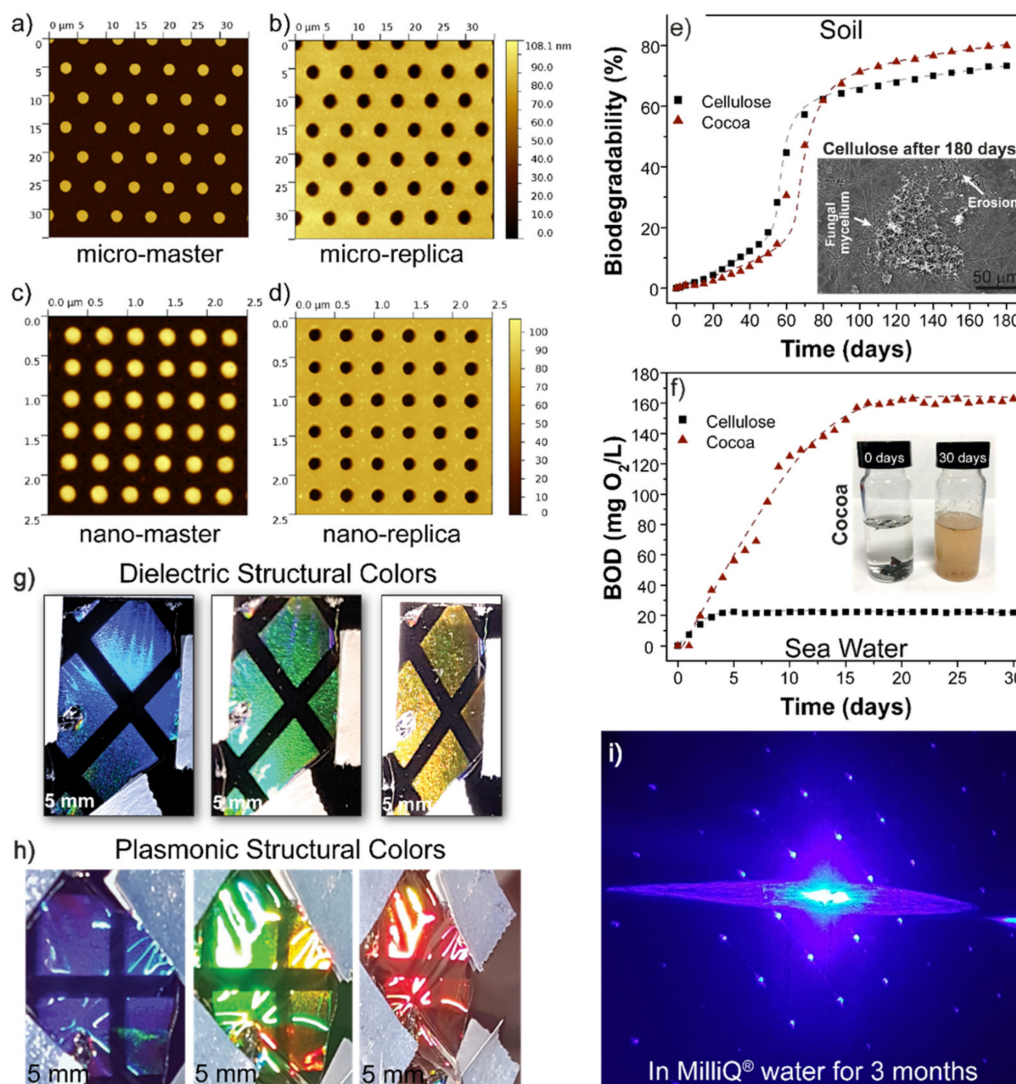

Figure 7. Cellulose Micro- and Nano-Devices: Solid-state micro- (**a**) and nano-scale (**c**) masters with the respective micro- (**b**) and nano-scale (**d**) cellulose replicae. Biodegradability in (**e**) soil and (**f**) sea water. (**g**) Dielectric and (**h**) plasmonic colors obtained by the structure in panel (**d**), for the dielectric case, and by the metallization of the same structure, for the plasmonic case. (**i**) Stability of the cellulose photonic crystal in panel (**b**) in MilliQ water for a three-month immersion. Reproduced with permission from reference [94]. [Copyright 2020, American Chemical Society].

3.3. Hydrogels

Hydrogels represent an exceptional bio-inspired alternative to classic non-biodegradable polymers for soft molding lithography. Their outstanding bio-compatibility makes them the material of choice for biological applications. Moreover, their broad customizability

in terms of mechanical and chemical properties makes them irreplaceable for tissue engineering, regenerative medicine and drug delivery [119–132]. Replica molding involving hydrogels is usually carried out by pouring a gel precursor over a solid-state master which is then immersed in the gelling agent [133]. However, improvements have been made to this technique by ensuring a controlled release of the gelling agent [132] (see Figure 8).
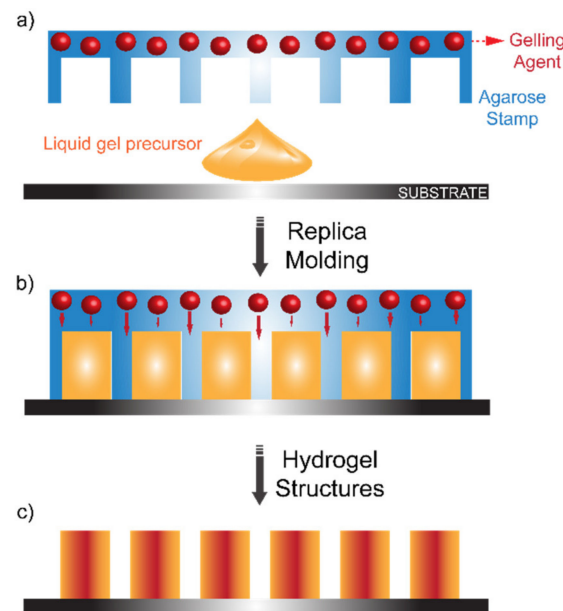

Figure 8. Hydrogel Replica Molding: (**a**) A liquid gel precursor is poured over a substrate. (**b**) An agarose stamp embedding the gelling agent is then positioned over the casted liquid gel precursor to carry out a classic replica-molding procedure. The gelling agent is gradually released. (c) Once the gellification process is complete, the agarose stamp is removed and the gellified structures are produced. Reproduced with permission from reference [132], copyright 2006, American Chemical Society.

Biocompatible photonic hydrogels based on elastin-like polymers have been used as genetically engineered stimuli-responsive photonic hydrogels [134–139]. Bovine serum albumin hydrogel-based micro-optics have been fabricated via direct laser writing [140]. Stimuli-responsive hydrogels have been used to modify the shape of a liquid droplet serving as a microlens, mounted over the hydrogel itself [141].

Silk-based hydrogels have been successfully employed to produce lenses for Light-Emitting Diodes with a light extraction efficiency of over 95% [142]. A micropatterned glucose-responsive hydrogel made of a glucose-responsive material (3-(acrylamido)-phenylboronic acid), crosslinked to acrylamide and deposited over a silica optical fiber, was shown to be effective for glucose detection [142].

Among the wide zoo of hydrogels available for the replica molding process, the agarose-based ones are worth mentioning. A micro-scale replica molding with agarose over a PDMS stamp has been demonstrated in 2004 by Mayer et al. [143]. Since then, optical devices such as planar waveguides or agarose-infiltrated optical fibers have been proposed [144–146].

4. Bio-Luminescent Gain Materials

On the photoluminescent material side (from this moment on, this review will use the terms "gain" and "photoluminescent" as synonyms), optimization could be carried out by intervening on the transition dipole moment of the molecule trying to maximize it. Such an approach is so powerful that, by using a high-transition-dipole moment molecule embedded in a cavity, it has recently been possible to reach an extremely strong light–matter interaction, usually called "ultra-strong coupling" regime, in which the coupling

strength between the discretized electromagnetic field of the cavity (playing the role of the light) and the excitons present in the molecule (playing the role of the matter) reached a value equal to a significant fraction of the energy of the molecular transition [147]. Considering such evident benefits, the always increasing research efforts toward the design of more performing dyes should not come as a surprise. It is true, however, that there have been numerous efforts to design inorganic semiconductor crystals such as Perovskites or Quantum Dots, which, in their most performing versions, owe their properties to the presence of Pb or Cd in their structure [148–159]. Such a feature makes them environmentally harmful.

On the other hand, it is well known that there are many large-dipole-moment molecules readily available in nature which can be used as the "active" core in our light-matter interaction scenario, in replacement of Cd- and Pb-based semiconductors [33,160]. Indeed, if we exclude inorganic semiconductors, fluorophores can be divided into two big categories: (i) intrinsic and (ii) extrinsic. Intrinsic fluorophores are those readily available in nature, while extrinsic ones are molecules whose photophysical, optical and chemical properties are customized to accomplish specific tasks, which are not addressable utilizing the intrinsic fluorophores. Intrinsic fluorophores can be bound to proteins to endow them with intrinsic fluorescence. For this reason, they are of special interest for this review, since they can represent the photoluminescent core of highly photoluminescent biological materials.

4.1. Intrinsic Fluorophores: Aromatic Amino Acids and Enzyme Cofactors

The photoluminescent core of intrinsic proteins is constituted by the fundamental aromatic amino acids: (i) tryptophan, (ii) tyrosine and (iii) phenylalanine. All of them manifest absorption and photoluminescence in the UV range. Phenylalanine is a monosubstituted benzene derivative, very similar to toluene. In phenylalanine, the bond between the phenyl group and the alanine partially destroys the symmetry of the benzene ring, opening symmetry-allowed transitions and, as a consequence, absorption and emission bands. Even though the transition dipole moment of phenylalanine is very low, understanding the origin of the photoluminescence of phenylalanine is fundamental to gain insight into more complex but yet very similar molecules. Tyrosine, for example, differs from phenylalanine by the presence of a hydroxylic group in the *para* position. The transition dipole moment of tyrosine is still small but slightly higher than that of phenylalanine. Tryptophan derives from indole, substituted in position C_3 with an alanine. As a consequence, its absorption properties stem from the high asymmetry of the indole molecule, where delocalized π electrons play a major role. Such a high asymmetry, together with incomplete delocalization of π electrons, generates a high dipole moment (3.4 D). Since the emission properties of tryptophan are highly influenced by the surrounding electromagnetic environment, tryptophan is largely used as an indicator of protein conformational change.

Apart from fundamental amino acids, enzyme cofactors can show a high photoluminescence as well. Two of the most known are nicotinamide adenine dinucleotide (NADH) and flavin adenine dinucleotide (FAD). Both are usually chemically bound to a protein, a process that dramatically increases their quantum yield [160–168]. Vitamins can also exhibit intrinsic photoluminescence. Pyridoxal phosphate, which is the active form of vitamin B6, is one of the most studied [169–177].

4.2. Aggregation-Induced Emission (AIE) Materials

Plenty of examples of bio-compatible and biodegradable high photoluminescent probes can be readily found in the framework of the so-called "aggregation-induced emission" (AIE) materials. Such kinds of composites are known to show no photoluminescence in their molecular form, but high photoemission upon aggregation [178–183]. These materials are highly interesting, since photoluminescent materials naturally tend to form aggregates, a process that usually proves detrimental for their photoluminescence. AIE was first observed by Luo et al. in 2001, when previously absent photoluminescence was enabled upon aggregation of 1-methyl-1.2.3.4.5-pentaphenylsilole [184]. Here,

Luo et al. observed that a freshly casted droplet of 1-methyl-1.2.3.4.5-pentaphenylsilole showed practically no photoluminescence, but it did while drying and, therefore, upon aggregation. From that moment, many examples of AIE have been provided, such as hydrocarbon luminogens [185], heteroatom-containing luminogens [186], luminogens with cyano substituents [187], luminogens with hydrogen bonds [188–190], polymeric luminogens [191,192], organometallic luminogens [193–196]. The capability of such molecules to manifest photoluminescence upon aggregation is somehow similar to a mechanism that will be discussed below, when we focus on a particular kind of new generation fluorophores called "Phytofluor". Indeed, the intramolecular rotations of aromatic rotors serve as a preferred non-radiative energy relaxation channel. Upon aggregation, such a mechanism is no more preferred due to cumbersome constraints. As a result, radiative channels open and bright photoluminescence arises [197]. One of the most interesting examples of a non-fluorescent protein whose luminescence is turned on via molecular aggregation is provided by the so-called "Green Fluorescent Protein" (GFP), a protein whose use in photonic technologies will be investigated shortly in this review. The chromophore of the GFP, a p-hydroxybenzylideneimidazolinone (p-HOBDI) molecule, is stored in an α-helix, surrounded, in turn, by a proteic β-Barrell. Such a spatially tight configuration does not allow the free rotation around the exo-methylene double bond, so that the only allowed relaxation channel for the chromophore is the radiative one that carries along the bright photoluminescence due to which GFP is so famous. Both denatured proteins or synthetic chromophores that cannot benefit from the steric hindrance of the β-Barrell suffer a tremendous quenching of the photoluminescence. However, upon aggregation, the restoration of the photoemissive properties has been recently demonstrated [198]. Of course, such a concept can be generalized to all those chemical configurations in which a molecular complex can modify the chromophore environment providing the necessary hindrance to disfavor the photo-isomerization of the molecule. For example, Debler et al. demonstrated that, when bound to the GFP chromophore, the antibody-stilbene complex provides the ideal steric condition to inhibit the photo-isomerization and unlock bright photoluminescence [199,200]. Such a technique is extremely promising for diagnostics purposes.

4.3. Fluorescent Proteins—Part A: Phycobiliproteins and Phytofluor

A special place in the realm of bio-inspired photoluminescent materials is occupied by proteins. Intense fluorescence can be expressed by Phycobiliproteins, whose emission range spans from blue to red [201–208]. Phycobiliproteins are capable of absorbing and harvesting the part of the light spectrum missed by chlorophyll and, as such, their absorbance spectra often peak around 470 nm to 650 nm. Their function is especially useful in water vegetable systems like algae, due to the weak penetration of short wavelengths in water. The capability of the phycobiliproteins to harvest light is highly enhanced by their elegant "antenna-like shape". Within the phycobilisomes (protein complexes in which phycobiliproteins are contained), phycobiliproteins are weakly emissive, but their photoluminescence dramatically increases upon their removal. Phycobiliproteins owe their photoluminescent properties to *bilins*, prosthetic groups consisting of open-chain tetrapyrrole groups, representing the covalently bound chromophores to the protein itself. There are four main phycobiliproteins: (i) Allophycocyanin, (ii) R-Phycocyanin, (iii) B-Phycoerythrin and (iv) R-Phycoerythrin. The large density of chromophores (bilins) present in phycobiliproteins is responsible for their exceptional photophysical properties. Phycobiliproteins have been recently successfully used as LASER dyes, in a classic Fabry–Pérot configuration [181].

An innovative family of bio-inspired fluorescent materials, that are attracting increasing interest, is the so-called "Phytofluors". Phytofluors are derived from phytochromes, a family of light-sensitive biliproteins that are very important for the adjustment of the living organism to environmental light conditions. Phytochromes are involved in vital processes of the plant which are not directly connected to photosynthesis, like seeds germination, leaves extension and flowering. The original phytochrome consists of a two-components

dimer: a chromophore and an apoprotein. The phytochrome chromophore belongs to the family of bilins (as in the case of the phycobiliproteins) and consists of an open-chain tetrapyrrole called phytochromobilin [202,209,210] (see Figure 9).
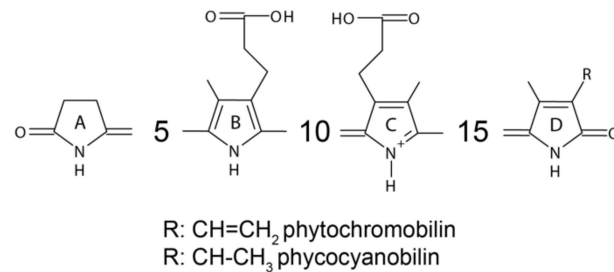

R: CH=CH$_2$ phytochromobilin
R: CH-CH$_3$ phycocyanobilin

Figure 9. Chemical structure of Phytochromobilin and Phycocyanobilin.

This chromophore optimizes the absorption of light by undergoing a trans-cis isomerization between the two configurations known as P$_r$ and P$_{fr}$. The former absorbs red light, while the latter absorbs in the near-infrared. The high efficiency of such a photoisomerization process prevents a high photoluminescence quantum yield of the chromophore as it is. Upon replacement of the natural bilin prosthetic group with phycoerythrobilin (PEB), the phytochrome turns into a highly fluorescent biliprotein. Such a process is favored by the fact that PEB spontaneously binds to the apoprotein of the phytochrome [202]. It has recently been reported that both the apoprotein and the chromophore itself can be expressed in *E. coli* bacteria, with the great advantage that, via a tyrosine-to-histidine mutation, the chromophore expressed in *E. coli* is readily fluorescent even though it lacks the trans-cis isomerization capability [211,212].

4.4. Fluorescent Proteins—Part B: Green Fluorescent Proteins and Similar

Talking about bioluminescent proteins, it is dutiful to reserve a place of honor to the famous green-fluorescent-protein (GFP). First isolated from *Aequorea Victoria* jellyfish (where the GFP is activated via a Förster Resonant Energy Transfer by a blue-emitting protein, namely the aequorin), the three-dimensional structure of the GFP (motif) is constituted by a distorted central α-helix protected by an 11-stranded β-barrel, where a chromophore responsible for the intense photoluminescence of the molecule is embedded [213–217]. The GFP can be represented as a nearly perfect cylinder with a diameter of about 2.5 nm and a height equal to 4 nm [218]. As expressed in the previous section, the GFP chromophore is made by three adjacent amino acids (Ser65, Gly67 and Tyr66), surrounded by a chemical environment made of amino acid residuals (see Figure 10a,b). The distorted α-helix protecting the chromophore is the key to favoring its folding in a photosensitive configuration, accessible to visible-light energies. Such a conformational state can be reached through a cyclization reaction in which an imidazole ring is formed (p-hydroxybenzylideneimidazolinone).

In the absence of the distortion induced by the α-helix, the molecule would reach a stable configuration by forming hydrogen bondings with the water molecules in the environment. This would imply additional energy to bring the molecule to its excited state, ruling out the possibility to carry out such a process via visible light.

The distorted shape of the α-helix, however, prevents the formation of hydrogen bondings, at the same time fostering the cyclization reaction. Such a process involves: (i) dehydration (Figure 10c), after which a very unstable reaction intermediate is produced and (ii) oxidation (Figure 10d), which concludes the cyclization, leading to the formation of a double ring [219]. In this state, the GFP chromophore is found in the so-called "protonated" form. When hit by a photon carrying an appropriate energy, the molecule is brought to an excited state characterized by an anionic form (Figure 10e).

The relaxation of the chromophore from its ionized state occurs via a process known as "excited state proton transfer" (ESPT), that can be largely influenced by the pH of the environment, determined by the amino acid residues. In fact, in its protonated form,

the pKa of the wild-type GFP chromophore in solution is rather alkaline (~ 8). After the excitation, the pKa decreases, assuming a value around 1. For this reason, the chromophore is deemed to be an awesome photoacid [218].
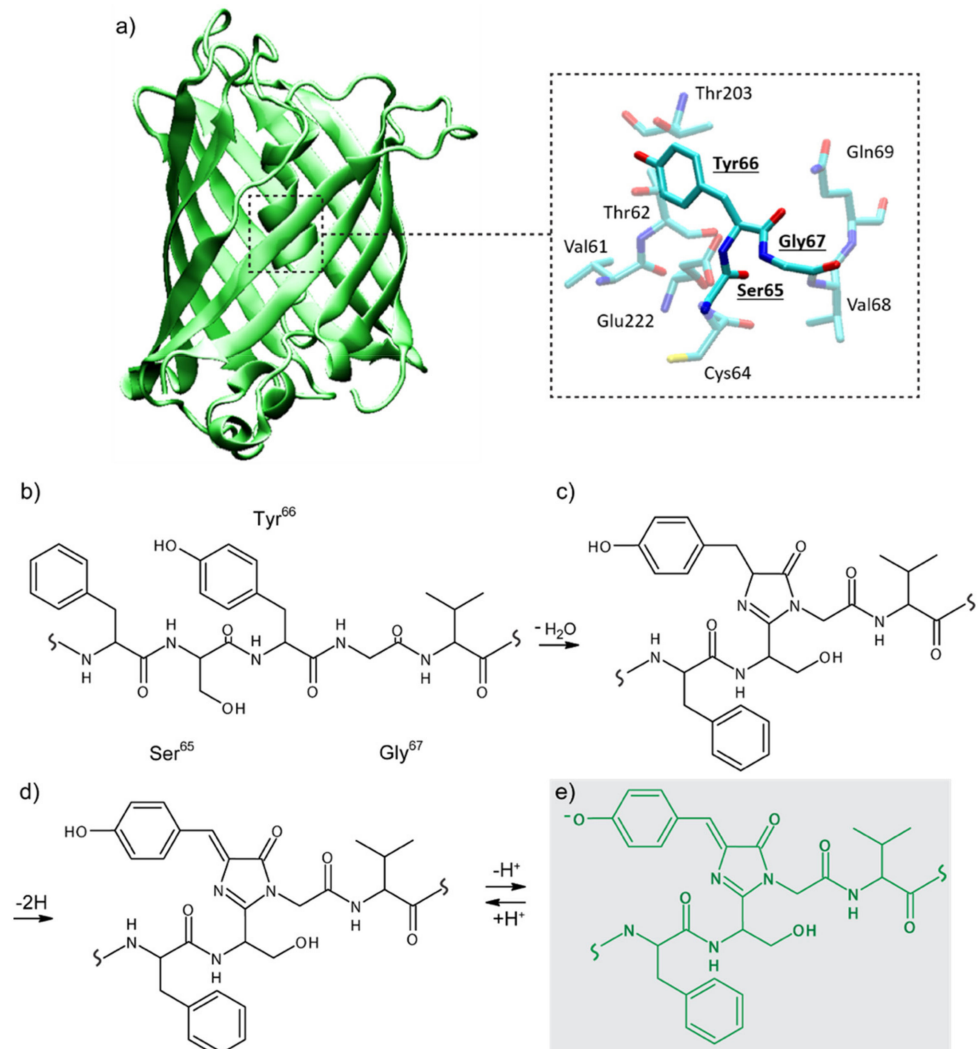

Figure 10. GFP structure and cyclization: (**a**) Structure of the GFP highlighting the β-barrel (green stripes) embedding the distorted α-helix. The chromophore, in the middle of the α-helix, is reported in the zoom. (**b–d**) Cyclization of the GFP chromophore starting from (**b**) the starting molecule which (**c**) undergoes a dehydration and (**d**) an oxidation process. The state plotted in (d) is the ground state or the "protonated" form of the chromophore. Upon excitation, the molecule brings itself into the so-called "anionic" state, plotted in (**e**).

GFP can be easily expressed in both prokaryotic and eukaryotic cells. It is common to see GFP expressed in *E. coli* bacteria, a configuration that lies at the core of many photonic applications, among which random and classic lasing, distributed feedback lasing, light-matter interaction and photonic entanglement [220–226]. The GFP is only one of the countless fluorescent proteins endowing organisms with bioluminescent properties. Such a broad choice allowed us to select blue-green-red triplets of photoemissive proteins to obtain white emitting diodes. One noticeable example of this has been reported by Weber et al., who used a blue (mTagBFP), green (eGFP) and red (mCherry) protein to form a white emitting gel, used as a light down-conversion coating [227]. Förster Resonant Energy Transfer (FRET) has been broadly reported between photoluminescent proteins [228]. FRET has been demonstrated between a large number of protein doublets, among which EGFP and tdTomato [229]. Some of the most popular FRET pairs are cyan-yellow fluorescent

protein pairs. Cyan donors like mTurquoise, mCerulean, mTFP1 and Aquamarine hold the great advantage of possessing very high quantum yields [230–239]. Typical acceptors to be coupled to cyan donors are variants of the Enhanced Yellow Fluorescent Proteins (EYFP) [239–242]. Red-green FRET pairs are common as well. On the green side, the GFP is the undisputed standard. Suitable red-emitting acceptors are mRuby derivatives, mGarnet and mCherry [243–248].

We report here a table (Table 2) summarizing the comparison of the transition dipole moment (tdm, expressed in Debye) of the molecular fluorophores (rhodamine, pyrromethene and coumarines) with those of some of the mentioned fluorescent proteins:

Table 2. Comparison of the transition dipole moment of the molecular fluorophores (rhodamine, pyrromethene and coumarines) with those of some of the reported fluorescent proteins.

Molecule	tdm (D)	Reference
Rhodamine 123	8.1	Chung et al. [249]
PM546	7.1	Chung et al. [249]
Coumarin (C153)	6.3	Uudesmaa et al. [250]
6MMC (Coumarin derivative)	6.4–9.8	Pandey et al. [251]
phiYFP	10.2	Nifosì et al. [252]
EYFP	10.1	Nifosì et al. [252]
Dronpa	10.46	Nifosì et al. [252]
GFP-S65T	10.5	Nifosì et al. [252]
mTFP0.7	9.915	Nifosì et al. [252]

5. Conclusions

Looking for a bio-inspired polaritonic framework in which to tailor an exceptional light–matter interaction, two main goals have to be pursued: (i) innovative resonant systems that provide the necessary "light" discretization and (ii) highly photoluminescent biological molecules as "matter" (exciton) reservoirs. It has been reported how architectures belonging to old-paradigm optoelectronics like Fabry–Pérot cavities are unsuitable to accomplish the first task, and a new kind of resonant meta-surfaces are readily available to replace them. Indeed, the field discretization occurring in meta-surfaces owes its properties only to the geometrical and structural distribution of the nanoelements by which the meta-surface is constituted. Such a planar character opens up to the replica-molding process applied to biodegradable polymers. Among the large zoo of meta-surface structures, we described two specific kinds of special interest under our perspective: (i) the so-called bi-periodic meta-surface and (ii) the ones sustaining symmetry-protected bound states in the continuum. Both of them can lead to high-Q-factor resonances and can be replicated via replica-molding processes in biopolymers. The second part of the review is, therefore, dedicated to mentioning some of the most remarkable bio-inspired polymers, which we think can be ideal to replicate meta-geometries toward biocompatible and biodegradable meta-surfaces, ready to host a biological gain material. Among these, we mentioned silk, cellulose and examples taken from the vast world of the hydrogels.

The third part of the review is dedicated to exploring some of the most intriguing and promising bioluminescent molecules, ready to be embedded in the biocompatible meta-surface. The simple but very important case of the aromatic enzymes, as well as two of the most important enzyme cofactors—NADH and FAD—have been described. Plant-derived fluorophores such as Phycobiliproteins and Phytofluors have been reported as a valid alternative to common extrinsic fluorescent probes, like rhodamines and coumarins. In the end, the noticeable example of fluorescent proteins like the green fluorescent protein has been analyzed, together with some of the most recent photonic and optoelectronic applications embedding them as a photoluminescent technological core.

As a perspective, this review envisions the merging of these two technologically advanced and mature worlds to enable the development of a new quantum framework in a fully biocompatible, biodegradable and bio-inspired scenario.

References

1. Fassioli, F.; Dinshaw, R.; Arpin, P.C.; Scholes, G.D. Photosynthetic Light Harvesting: Excitons and Coherence. *J. R. Soc. Interface* **2014**, *11*, 20130901. [CrossRef] [PubMed]
2. Kittel, C. *Introduction to Solid State Physics*, 7th ed.; Wiley, J., Ed.; Wiley: Hoboken, NJ, USA, 1996; ISBN 978-0471415268.
3. Snoke, D.W. *Solid State Physics*; Cambridge University Press: Cambridge, UK, 2020; ISBN 9781108123815.
4. Einstein, A. Über Einen Die Erzeugung Und Verwandlung Des Lichtes Betreffenden Heuristischen Gesichtspunkt. *Ann. Der Phys.* **1905**, *322*, 132–148. [CrossRef]
5. Scully, M.O.; Zubairy, M.S. *Quantum Optics*; Cambridge University Press: Cambridge, UK, 1997; p. 630. ISBN 0521434580.
6. Kasap, S.O. *Optoelectronics and Photonics: Principles and Practices*; Prentice Hall: Hoboken, NJ, USA, 2001; p. 340. ISBN 9780201610871.
7. Born, M.; Wolf, E. *Principles of Optics Electromagnetic Theory of Propagation, Interference and Diffraction of Light*; Pergamon Press: Oxford, UK, 1980; p. 952. ISBN 0521642221.
8. Jacob, Z.; Smolyaninov, I.I.; Narimanov, E.E. Broadband Purcell Effect: Radiative Decay Engineering with Metamaterials. *Appl. Phys. Lett.* **2012**, *100*, 181105. [CrossRef]
9. Jahani, S.; Zhao, H.; Jacob, Z. Switching Purcell Effect with Nonlinear Epsilon-near-Zero Media. *Appl. Phys. Lett.* **2018**, *113*, 021103. [CrossRef]
10. Akselrod, G.M.; Argyropoulos, C.; Hoang, T.B.; Ciracì, C.; Fang, C.; Huang, J.; Smith, D.R.; Mikkelsen, M.H. Probing the Mechanisms of Large Purcell Enhancement in Plasmonic Nanoantennas. *Nat. Photonics* **2014**, *8*, 835–840. [CrossRef]
11. Lu, Y.J.; Sokhoyan, R.; Cheng, W.H.; Shirmanesh, G.K.; Davoyan, A.R.; Pala, R.A.; Thyagarajan, K.; Atwater, H.A. Dynamically Controlled Purcell Enhancement of Visible Spontaneous Emission in a Gated Plasmonic Heterostructure. *Nat. Commun.* **2017**, *8*, 1631. [CrossRef]
12. Caligiuri, V.; Palei, M.; Imran, M.; Manna, L.; Krahne, R. Planar Double-Epsilon-Near-Zero Cavities for Spontaneous Emission and Purcell Effect Enhancement. *ACS Photonics* **2018**, *5*, 2287–2294. [CrossRef]
13. Jeantet, A.; Chassagneux, Y.; Raynaud, C.; Roussignol, P.; Lauret, J.S.; Besga, B.; Estève, J.; Reichel, J.; Voisin, C. Widely Tunable Single-Photon Source from a Carbon Nanotube in the Purcell Regime. *Phys. Rev. Lett.* **2016**, *116*, 247402–247407. [CrossRef]
14. Purcell, E.M. Spontaneous Emission Probabilities at Radio Frequencies. *Proc. Am. Phys. Soc.* **1946**, *69*, 681.
15. Kristensen, P.T.; Van Vlack, C.; Hughes, S. Generalized Effective Mode Volume for Leaky Optical Cavities. *Opt. Lett.* **2012**, *37*, 1649. [CrossRef] [PubMed]
16. Muljarov, E.A.; Langbein, W. Exact Mode Volume and Purcell Factor of Open Optical Systems. *Phys. Rev. B* **2016**, *94*, 235438. [CrossRef]
17. Coccioli, R.; Boroditsky, M.; Kim, K.W.; Rahmat-Samii, Y.; Yablonovitch, E. Smallest Possible Electromagnetic Mode Volume in a Dielectric Cavity. *IEE Proc. Optoelectron.* **1998**, *145*, 391–396. [CrossRef]
18. Li, X.; Smalley, J.S.T.; Li, Z.; Gu, Q. Effective Modal Volume in Nanoscale Photonic and Plasmonic Near-Infrared Resonant Cavities. *Appl. Sci.* **2018**, *8*, 1464. [CrossRef]
19. Gao, J.; McMillan, J.F.; Wu, M.-C.; Zheng, J.; Assefa, S.; Wong, C.W. Demonstration of an Air-Slot Mode-Gap Confined Photonic Crystal Slab Nanocavity with Ultrasmall Mode Volumes. *Appl. Phys. Lett.* **2010**, *96*, 051123. [CrossRef]
20. Bahari, B.; Tellez-Limon, R.; Kante, B. Directive and Enhanced Spontaneous Emission Using Shifted Cubes Nanoantenna. *J. Appl. Phys.* **2016**, *120*, 093106. [CrossRef]
21. Nezhad, M.P.; Simic, A.; Bondarenko, O.; Slutsky, B.; Mizrahi, A.; Feng, L.; Lomakin, V.; Fainman, Y. Room-Temperature Subwavelength Metallo-Dielectric Lasers. *Nature Photonics* **2010**, *4*, 395–399. [CrossRef]
22. Gérard, J.M.; Gayral, B. Strong Purcell Effect for InAs Quantum Boxes in Three-Dimensional Solid-State Microcavities. *J. Lightwave Technol.* **1999**, *17*, 2089–2095. [CrossRef]
23. Zhang, L.; Gogna, R.; Burg, W.; Tutuc, E.; Deng, H. Photonic-Crystal Exciton-Polaritons in Monolayer Semiconductors. *Nat. Commun.* **2018**, *9*, 713. [CrossRef]
24. Plumhof, J.D.; Stöferle, T.; Mai, L.; Scherf, U.; Mahrt, R.F. Room-Temperature Bose-Einstein Condensation of Cavity Exciton-Polaritons in a Polymer. *Nat. Mater.* **2014**, *13*, 247–252. [CrossRef]

25. Skolnick, M.S.; Fisher, T.A.; Whittaker, D.M. Strong Coupling Phenomena in Quantum Microcavity Structures. *Semicond. Sci. Technol.* **1998**, *13*, 645–669. [CrossRef]

26. Lidzey, D.G.; Bradley, D.D.C.; Skolnick, M.S.; Virgili, T.; Walker, S.; Whittaker, D.M. Strong Exciton-Photon Coupling in an Organic Semiconductor Microcavity. *Nature* **1998**, *395*, 53–55. [CrossRef]

27. Hennessy, K.; Badolato, A.; Winger, M.; Gerace, D.; Atatüre, M.; Gulde, S.; Fält, S.; Hu, E.L.; Imamoğlu, A. Quantum Nature of a Strongly Coupled Single Quantum Dot-Cavity System. *Nature* **2007**, *445*, 896–899. [CrossRef]

28. Houdré, R.; Stanley, R.P.; Oesterle, U.; Ilegems, M.; Weisbuch, C. Room-Temperature Cavity Polaritons in a Semiconductor Microcavity. *Phys. Rev. B* **1994**, *49*, 16761–16764. [CrossRef] [PubMed]

29. Carusotto, I.; Ciuti, C. Quantum Fluids of Light. *Rev. Mod. Phys.* **2013**, *85*, 299–366. [CrossRef]

30. Yoshle, T.; Scherer, A.; Hendrickson, J.; Khitrova, G.; Gibbs, H.M.; Rupper, G.; Ell, C.; Shchekin, O.B.; Deppe, D.G. Vacuum Rabi Splitting with a Single Quantum Dot in a Photonic Crystal Nanocavity. *Nature* **2004**, *432*, 200–203. [CrossRef]

31. Coppolaro, M.; Moccia, M.; Castaldi, G.; Alu, A.; Galdi, V. Surface-Wave Propagation on Non-Hermitian Metasurfaces with Extreme Anisotropy. *IEEE Trans. Microw. Theory Tech.* **2021**, *69*, 2060–2071. [CrossRef]

32. Chen, W.T.; Zhu, A.Y.; Capasso, F. Flat Optics with Dispersion-Engineered Metasurfaces. *Nat. Rev. Mater.* **2020**, *5*, 604–620. [CrossRef]

33. Di Meo, V.; Moccia, M.; Sanità, G.; Crescitelli, A.; Lamberti, A.; Galdi, V.; Rendina, I.; Esposito, E. Advanced DNA Detection via Multispectral Plasmonic Metasurfaces. *Front. Bioeng. Biotechnol.* **2021**, *9*, 666121. [CrossRef]

34. Yu, N.; Genevet, P.; Kats, M.A.; Aieta, F.; Tetienne, J.-P.; Capasso, F.; Gaburro, Z. Light Propagation with Phase Discontinuities: Generalized Laws of Reflection and Refraction. *Science* **2011**, *334*, 333–337. [CrossRef] [PubMed]

35. Shaltout, A.M.; Shalaev, V.M.; Brongersma, M.L. Spatiotemporal Light Control with Active Metasurfaces. *Science* **2019**, *364*, 298–302. [CrossRef]

36. Krasnok, A.; Tymchenko, M.; Alù, A. Nonlinear Metasurfaces: A Paradigm Shift in Nonlinear Optics. *Mater. Today* **2018**, *21*, 8–21. [CrossRef]

37. Wu, P.C.; Tsai, W.-Y.; Chen, W.T.; Huang, Y.-W.; Chen, T.-Y.; Chen, J.-W.; Liao, C.Y.; Chu, C.H.; Sun, G.; Tsai, D.P. Versatile Polarization Generation with an Aluminum Plasmonic Metasurface. *Nano Lett.* **2016**, *17*, 445–452. [CrossRef]

38. Caligiuri, V.; De Sio, L.; Petti, L.; Capasso, R.; Rippa, M.; Maglione, M.G.; Tabiryan, N.; Umeton, C. Electro-/All-Optical Light Extraction in Gold Photonic Quasi-Crystals Layered with Photosensitive Liquid Crystals. *Adv. Opt. Mater.* **2014**, *2*, 950–955. [CrossRef]

39. Kamali, S.M.; Arbabi, E.; Arbabi, A.; Faraon, A. A Review of Dielectric Optical Metasurfaces for Wavefront Control. *Nanophotonics* **2018**, *7*, 1041–1068. [CrossRef]

40. Ding, F.; Pors, A.; Bozhevolnyi, S.I. Gradient Metasurfaces: A Review of Fundamentals and Applications. *Rep. Prog. Phys.* **2017**, *81*, 026401. [CrossRef]

41. Kruk, S.; Kivshar, Y. Functional Meta-Optics and Nanophotonics Governed by Mie Resonances. *ACS Photonics* **2017**, *4*, 2638–2649. [CrossRef]

42. Mueller, J.P.B.; Rubin, N.A.; Devlin, R.C.; Groever, B.; Capasso, F.; Paulson, J.A. Metasurface Polarization Optics: Independent Phase Control of Arbitrary Orthogonal States of Polarization. *Phys. Rev. Lett.* **2017**, *118*, 113901. [CrossRef] [PubMed]

43. Wang, S.; Wu, P.C.; Su, V.-C.; Lai, Y.-C.; Chu, C.H.; Chen, J.-W.; Lu, S.-H.; Chen, J.; Xu, B.; Kuan, C.-H.; et al. Broadband Achromatic Optical Metasurface Devices. *Nature Commun.* **2017**, *8*, 187. [CrossRef]

44. Lininger, A.; Zhu, A.Y.; Park, J.-S.; Palermo, G.; Chatterjee, S.; Boyd, J.; Capasso, F.; Strangi, G. Optical Properties of Metasurfaces Infiltrated with Liquid Crystals. *Proc. Natl. Acad. Sci. USA* **2020**, *117*, 20390–20396. [CrossRef] [PubMed]

45. Tuz, V.R.; Khardikov, V.V.; Kivshar, Y.S. All-Dielectric Resonant Metasurfaces with a Strong Toroidal Response. *ACS Photonics* **2018**, *5*, 1871–1876. [CrossRef]

46. Santiago-Cruz, T.; Fedotova, A.; Sultanov, V.; Weissflog, M.A.; Arslan, D.; Younesi, M.; Pertsch, T.; Staude, I.; Setzpfandt, F.; Chekhova, M. Photon Pairs from Resonant Metasurfaces. *Nano Lett.* **2021**, *21*, 4429. [CrossRef]

47. Zou, C.; Sautter, J.; Setzpfandt, F.; Staude, I. Resonant Dielectric Metasurfaces: Active Tuning and Nonlinear Effects. *J. Phys. D Appl. Phys.* **2019**, *52*, 373002. [CrossRef]

48. Kuznetsov, A.I.; Miroshnichenko, A.E.; Brongersma, M.L.; Kivshar, Y.S.; Luk'yanchuk, B. Optically Resonant Dielectric Nanostructures. *Science* **2016**, *354*, aag2472. [CrossRef] [PubMed]

49. Staude, I.; Pertsch, T.; Kivshar, Y.S. All-Dielectric Resonant Meta-Optics Lightens Up. *ACS Photonics* **2019**, *6*, 802–814. [CrossRef]

50. Pertsch, T.; Kivshar, Y. Nonlinear Optics with Resonant Metasurfaces. *MRS Bull.* **2020**, *45*, 210–220. [CrossRef]

51. Overvig, A.; Alù, A. Wavefront-Selective Fano Resonant Metasurfaces. *Adv. Photonics* **2021**, *3*, 026002. [CrossRef]

52. Zubyuk, V.; Carletti, L.; Shcherbakov, M.; Kruk, S. Resonant Dielectric Metasurfaces in Strong Optical Fields. *APL Mater.* **2021**, *9*, 60701. [CrossRef]

53. Sadrieva, Z.F.; Sinev, I.S.; Koshelev, K.L.; Samusev, A.; Iorsh, I.V.; Takayama, O.; Malureanu, R.; Bogdanov, A.A.; Lavrinenko, A.V. Transition from Optical Bound States in the Continuum to Leaky Resonances: Role of Substrate and Roughness. *ACS Photonics* **2017**, *4*, 723–727. [CrossRef]

54. Koshelev, K.; Favraud, G.; Bogdanov, A.; Kivshar, Y.; Fratalocchi, A. Nonradiating Photonics with Resonant Dielectric Nanostructures. *Nanophotonics* **2019**, *8*, 725–745. [CrossRef]

55. Doeleman, H.M.; Monticone, F.; Den Hollander, W.; Alù, A.; Koenderink, A.F. Experimental Observation of a Polarization Vortex at an Optical Bound State in the Continuum. *Nat. Photonics* **2018**, *12*, 397–401. [CrossRef]

56. Carletti, L.; Koshelev, K.; De Angelis, C.; Kivshar, Y. Giant Nonlinear Response at the Nanoscale Driven by Bound States in the Continuum. *Phys. Rev. Lett.* **2018**, *121*, 033903. [CrossRef]

57. Yesilkoy, F.; Arvelo, E.R.; Jahani, Y.; Liu, M.; Tittl, A.; Cevher, V.; Kivshar, Y.; Altug, H. Ultrasensitive Hyperspectral Imaging and Biodetection Enabled by Dielectric Metasurfaces. *Nat. Photonics* **2019**, *13*, 390–396. [CrossRef]

58. Ha, S.T.; Fu, Y.H.; Emani, N.K.; Pan, Z.; Bakker, R.M.; Paniagua-Domínguez, R.; Kuznetsov, A.I. Directional Lasing in Resonant Semiconductor Nanoantenna Arrays. *Nat. Nanotechnol.* **2018**, *13*, 1042–1047. [CrossRef]

59. Rybin, M.V.; Koshelev, K.L.; Sadrieva, Z.F.; Samusev, K.B.; Bogdanov, A.A.; Limonov, M.F.; Kivshar, Y.S. High-Q Supercavity Modes in Subwavelength Dielectric Resonators. *Phys. Rev. Lett.* **2017**, *119*, 243901. [CrossRef]

60. Koshelev, K.; Lepeshov, S.; Liu, M.; Bogdanov, A.; Kivshar, Y. Asymmetric Metasurfaces with High-Q Resonances Governed by Bound States in the Continuum. *Phys. Rev. Lett.* **2018**, *121*, 193903. [CrossRef] [PubMed]

61. Kodigala, A.; Lepetit, T.; Gu, Q.; Bahari, B.; Fainman, Y.; Kanté, B. Lasing Action from Photonic Bound States in Continuum. *Nature* **2017**, *541*, 196–199. [CrossRef] [PubMed]

62. Hu, J.; Lawrence, M.; Dionne, J.A. High Quality Factor Dielectric Metasurfaces for Ultraviolet Circular Dichroism Spectroscopy. *ACS Photonics* **2020**, *7*, 36–42. [CrossRef]

63. Han, S.; Cong, L.; Srivastava, Y.K.; Qiang, B.; Rybin, M.V.; Kumar, A.; Jain, R.; Lim, W.X.; Achanta, V.G.; Prabhu, S.S.; et al. All-Dielectric Active Terahertz Photonics Driven by Bound States in the Continuum. *Adv. Mater.* **2019**, *31*, 1901921. [CrossRef]

64. He, Y.; Guo, G.; Feng, T.; Xu, Y.; Miroshnichenko, A.E. Toroidal Dipole Bound States in the Continuum. *Phys. Rev. B* **2018**, *98*, 161112. [CrossRef]

65. Gomis-Bresco, J.; Artigas, D.; Torner, L. Anisotropy-Induced Photonic Bound States in the Continuum. *Nature Photonics* **2017**, *11*, 232–236. [CrossRef]

66. Koshelev, K.; Bogdanov, A.; Kivshar, Y. Meta-Optics and Bound States in the Continuum. *Sci. Bull.* **2019**, *64*, 836–842. [CrossRef]

67. Azzam, S.I.; Shalaev, V.M.; Boltasseva, A.; Kildishev, A.V. Formation of Bound States in the Continuum in Hybrid Plasmonic-Photonic Systems. *Phys. Rev. Lett.* **2018**, *121*, 253901. [CrossRef]

68. Jin, J.; Yin, X.; Ni, L.; Soljačić, M.; Zhen, B.; Peng, C. Topologically Enabled Ultrahigh-Q Guided Resonances Robust to out-of-Plane Scattering. *Nature* **2019**, *574*, 501–504. [CrossRef] [PubMed]

69. Von Neuman, J.; Wigner, E.; von Neuman, J.; Wigner, E. Uber Merkwürdige Diskrete Eigenwerte. Uber Das Verhalten von Eigenwerten Bei Adiabatischen Prozessen. *PhyZ* **1929**, *30*, 467–470.

70. Friedrich, H.; Wintgen, D. Interfering Resonances and Bound States in the Continuum. *Phys. Rev. A* **1985**, *32*, 3231. [CrossRef]

71. Hsu, C.W.; Zhen, B.; Stone, A.D.; Joannopoulos, J.D.; Soljačić, M. Bound States in the Continuum. *Nature Rev. Mater.* **2016**, *1*, 16048. [CrossRef]

72. Tittl, A.; Leitis, A.; Liu, M.; Yesilkoy, F.; Choi, D.-Y.; Neshev, D.N.; Kivshar, Y.S.; Altug, H. Imaging-Based Molecular Barcoding with Pixelated Dielectric Metasurfaces. *Science* **2018**, *360*, 1105–1109. [CrossRef]

73. Xia, Y.; Whitesides, G.M. Soft Lithography. *Annu. Rev. Mater. Sci.* **1998**, *28*, 153–184. [CrossRef]

74. Qin, D.; Xia, Y.; Whitesides, G.M. Soft Lithography for Micro- and Nanoscale Patterning. *Nat. Protoc.* **2010**, *5*, 491–502. [CrossRef] [PubMed]

75. Ahadian, S.; Civitarese, R.; Bannerman, D.; Mohammadi, M.H.; Lu, R.; Wang, E.; Davenport-Huyer, L.; Lai, B.; Zhang, B.; Zhao, Y.; et al. Organ-On-A-Chip Platforms: A Convergence of Advanced Materials, Cells, and Microscale Technologies. *Adv. Healthc. Mater.* **2018**, *7*, 1700506. [CrossRef] [PubMed]

76. Yuk, H.; Lu, B.; Lin, S.; Qu, K.; Xu, J.; Luo, J.; Zhao, X. 3D Printing of Conducting Polymers. *Nat. Commun.* **2020**, *11*, 1604. [CrossRef]

77. Cataldi, U.; Caputo, R.; Kurylyak, Y.; Klein, G.; Chekini, M.; Umeton, C.; Bürgi, T. Growing Gold Nanoparticles on a Flexible Substrate to Enable Simple Mechanical Control of Their Plasmonic Coupling. *J. Mater. Chem. C* **2014**, *2*, 7927–7933. [CrossRef]

78. Wolf, M.P.; Salieb-Beugelaar, G.B.; Hunziker, P. PDMS with Designer Functionalities—Properties, Modifications Strategies, and Applications. *Prog. Polym. Sci.* **2018**, *83*, 97–134. [CrossRef]

79. Wang, Z.; Ma, Z.; Sun, J.; Yan, Y.; Bu, M.; Huo, Y.; Li, Y.-F.; Hu, N. Recent Advances in Natural Functional Biopolymers and Their Applications of Electronic Skins and Flexible Strain Sensors. *Polymers* **2021**, *13*, 813. [CrossRef]

80. Campbell, S.B.; Wu, Q.; Yazbeck, J.; Liu, C.; Okhovatian, S.; Radisic, M. Beyond Polydimethylsiloxane: Alternative Materials for Fabrication of Organ-on-a-Chip Devices and Microphysiological Systems. *ACS Biomater. Sci. Eng.* **2020**, *7*, 2880–2899. [CrossRef]

81. Shan, D.; Gerhard, E.; Zhang, C.; Tierney, J.W.; Xie, D.; Liu, Z.; Yang, J. Polymeric Biomaterials for Biophotonic Applications. *Bioact. Mater.* **2018**, *3*, 434–445. [CrossRef]

82. Omenetto, F.G.; Kaplan, D.L. A New Route for Silk. *Nat. Photonics* **2008**, *2*, 641–643. [CrossRef]

83. Guidetti, G.; Wang, Y.; Omenetto, F.G. Active Optics with Silk. *Nanophotonics* **2020**, *10*, 137–148. [CrossRef]

84. Rockwood, D.N.; Preda, R.C.; Yücel, T.; Wang, X.; Lovett, M.L.; Kaplan, D.L. Materials Fabrication from Bombyx Mori Silk Fibroin. *Nature Protoc.* **2011**, *6*, 1612–1631. [CrossRef]

85. Bettinger, C.J.; Cyr, K.M.; Matsumoto, A.; Langer, R.; Borenstein, J.T.; Kaplan, D.L. Silk Fibroin Microfluidic Devices. *Adv. Mater.* **2007**, *19*, 2847–2850. [CrossRef] [PubMed]

86.　Xu, M.; Pradhan, S.; Agostinacchio, F.; Pal, R.K.; Greco, G.; Mazzolai, B.; Pugno, N.M.; Motta, A.; Yadavalli, V.K. Easy, Scalable, Robust, Micropatterned Silk Fibroin Cell Substrates. *Adv. Mater. Interfaces* **2019**, *6*, 1801822. [CrossRef]

87.　Pal, R.K.; Kurland, N.E.; Wang, C.; Kundu, S.C.; Yadavalli, V.K. Biopatterning of Silk Proteins for Soft Micro-Optics. *ACS Appl. Mater. Interfaces* **2015**, *7*, 8809–8816. [CrossRef] [PubMed]

88.　Wang, Y.; Aurelio, D.; Li, W.; Tseng, P.; Zheng, Z.; Li, M.; Kaplan, D.L.; Liscidini, M.; Omenetto, F.G. Modulation of Multiscale 3D Lattices through Conformational Control: Painting Silk Inverse Opals with Water and Light. *Adv. Mater.* **2017**, *29*, 1702769. [CrossRef]

89.　Li, W.; Wang, Y.; Li, M.; Garbarini, L.P.; Omenetto, F.G. Inkjet Printing of Patterned, Multispectral, and Biocompatible Photonic Crystals. *Adv. Mater.* **2019**, *31*, 1901036. [CrossRef] [PubMed]

90.　Kim, S.; Marelli, B.; Brenckle, M.A.; Mitropoulos, A.N.; Gil, E.S.; Tsioris, K.; Tao, H.; Kaplan, D.L.; Omenetto, F.G. All-Water-Based Electron-Beam Lithography Using Silk as a Resist. *Nat. Nanotechnol.* **2014**, *9*, 306–310. [CrossRef]

91.　Klemm, D.; Heublein, B.; Fink, H.P.; Bohn, A. Cellulose: Fascinating Biopolymer and Sustainable Raw Material. *Angew. Chem. Int. Ed.* **2005**, *44*, 3358–3393. [CrossRef]

92.　*Ullmann's Encyclopedia of Industrial Chemistry*; Wiley: Hoboken, NJ, USA, 2000.

93.　Bayer, I.S.; Guzman-Puyol, S.; Heredia-Guerrero, J.A.; Ceseracciu, L.; Pignatelli, F.; Ruffilli, R.; Cingolani, R.; Athanassiou, A. Direct Transformation of Edible Vegetable Waste into Bioplastics. *Macromolecules* **2014**, *47*, 5135–5143. [CrossRef]

94.　Caligiuri, V.; Tedeschi, G.; Palei, M.; Miscuglio, M.; Martin-Garcia, B.; Guzman-Puyol, S.; Hedayati, M.K.; Kristensen, A.; Athanassiou, A.; Cingolani, R.; et al. Biodegradable and Insoluble Cellulose Photonic Crystals and Metasurfaces. *ACS Nano* **2020**, *14*, 9502–9511. [CrossRef] [PubMed]

95.　Espinha, A.; Dore, C.; Matricardi, C.; Alonso, M.I.; Goñi, A.R.; Mihi, A. Hydroxypropyl Cellulose Photonic Architectures by Soft Nanoimprinting Lithography. *Nat. Photonics* **2018**, *12*, 343–348. [CrossRef]

96.　Ryabchun, A.; Bobrovsky, A. Cholesteric Liquid Crystal Materials for Tunable Diffractive Optics. *Adv. Opt. Mater.* **2018**, *6*, 1800335. [CrossRef]

97.　Mitov, M. Cholesteric Liquid Crystals in Living Matter. *Soft Matter* **2017**, *13*, 4176–4209. [CrossRef] [PubMed]

98.　Finkelmann, H.; Kim, S.T.; Muaeoz, A.; Palffy-Muhoray, P.; Taheri, B. Tunable Mirrorless Lasing in Cholesteric Liquid Crystalline Elastomers. *Adv. Mater.* **2001**, *13*, 1069–1072. [CrossRef]

99.　Green, M.M.; Peterson, N.C.; Sato, T.; Teramoto, A.; Cook, R.; Lifson, S. A Helical Polymer with a Cooperative Response to Chiral Information. *Science* **1995**, *268*, 1860–1866. [CrossRef] [PubMed]

100.　Chilaya, G.; Chanishvili, A.; Petriashvili, G.; Barberi, R.; Bartolino, R.; De Santo, M.P.; Matranga, M.A.; Collings, P. Light Control of Cholesteric Liquid Crystals Using Azoxy-Based Host Materials. *Mol. Cryst. Liq. Cryst.* **2006**, *453*, 123–140. [CrossRef]

101.　Chanishvili, A.; Chilaya, G.; Petriashvili, G.; Barberi, R.; Bartolino, R.; Cipparrone, G.; Mazzulla, A. Laser Emission from a Dye-Doped Cholesteric Liquid Crystal Pumped by Another Cholesteric Liquid Crystal Laser. *Appl. Phys. Lett.* **2004**, *85*, 3378–3380. [CrossRef]

102.　Frka-Petesic, B.; Vignolini, S. So Much More than Paper. *Nat. Photonics* **2019**, *13*, 365–367. [CrossRef]

103.　Habibi, Y.; Lucia, L.A.; Rojas, O.J. Cellulose Nanocrystals: Chemistry, Self-Assembly, and Applications. *Chem. Rev.* **2010**, *110*, 3479–3500. [CrossRef]

104.　Kontturi, E.; Laaksonen, P.; Linder, M.B.; Nonappa; Gröschel, A.H.; Rojas, O.J.; Ikkala, O. Advanced Materials through Assembly of Nanocelluloses. *Adv. Mater.* **2018**, *30*, 1703779. [CrossRef] [PubMed]

105.　Arcot, L.R.; Gröschel, A.H.; Linder, M.B.; Rojas, O.J.; Ikkala, O. Self-Assembly of Native Cellulose Nanostructures. In *Handbook of Nanocellulose and Cellulose Nanocomposites*; Wiley-VCH: Hoboken, NJ, USA, 2017; pp. 123–174.

106.　Kargarzadeh, H.; Ioelovich, M.; Ahmad, I.; Thomas, S.; Dufresne, A. Methods for Extraction of Nanocellulose from Various Sources. In *Handbook of Nanocellulose and Cellulose Nanocomposites*; Wiley-VCH: Hoboken, NJ, USA, 2017; pp. 1–49.

107.　Klemm, D.; Kramer, F.; Moritz, S.; Lindström, T.; Ankerfors, M.; Gray, D.; Dorris, A. Nanocelluloses: A New Family of Nature-Based Materials. *Angew. Chem. Int. Ed.* **2011**, *50*, 5438–5466. [CrossRef] [PubMed]

108.　Honorato-Rios, C.; Bruckner, J.; Schütz, C.; Wagner, S.; Tosheva, Z.; Bergström, L.; Lagerwall, J.P.F. Cholesteric liquid crystal formation in suspensions of cellulose nanocrystals. In *Liquid Crystals with Nano and Microparticles*; World Scientific Publishing Co. Pte. Ltd.: Singapore, 2016; Volume 2, pp. 871–897. ISBN 9789814619264.

109.　Beck, S.; Méthot, M.; Bouchard, J. General Procedure for Determining Cellulose Nanocrystal Sulfate Half-Ester Content by Conductometric Titration. *Cellulose* **2015**, *22*, 101–116. [CrossRef]

110.　Abitbol, T.; Kloser, E.; Gray, D.G. Estimation of the Surface Sulfur Content of Cellulose Nanocrystals Prepared by Sulfuric Acid Hydrolysis. *Cellulose* **2013**, *20*, 785–794. [CrossRef]

111.　Revol, J.F.; Bradford, H.; Giasson, J.; Marchessault, R.H.; Gray, D.G. Helicoidal Self-Ordering of Cellulose Microfibrils in Aqueous Suspension. *Int. J. Biol. Macromol.* **1992**, *14*, 170–172. [CrossRef]

112.　Kadar, R.; Spirk, S.; Nypelo, T. Cellulose Nanocrystal Liquid Crystal Phases: Progress and Challenges in Characterization Using Rheology Coupled to Optics, Scattering, and Spectroscopy. *ACS Nano* **2021**, *15*, 7931–7945. [CrossRef] [PubMed]

113.　Schütz, C.; Bruckner, J.R.; Honorato-Rios, C.; Tosheva, Z.; Anyfantakis, M.; Lagerwall, J.P.F. From Equilibrium Liquid Crystal Formation and Kinetic Arrest to Photonic Bandgap Films Using Suspensions of Cellulose Nanocrystals. *Crystals* **2020**, *10*, 199. [CrossRef]

114. Wang, P.X.; Hamad, W.Y.; MacLachlan, M.J. Polymer and Mesoporous Silica Microspheres with Chiral Nematic Order from Cellulose Nanocrystals. *Angew. Chem. Int. Ed.* **2016**, *55*, 12460–12464. [CrossRef] [PubMed]

115. Hirai, A.; Inui, O.; Horii, F.; Tsuji, M. Phase Separation Behavior in Aqueous Suspensions of Bacterial Cellulose Nanocrystals Prepared by Sulfuric Acid Treatment. *Langmuir* **2009**, *25*, 497–502. [CrossRef]

116. Wang, P.X.; Hamad, W.Y.; MacLachlan, M.J. Structure and Transformation of Tactoids in Cellulose Nanocrystal Suspensions. *Nat. Commun.* **2016**, *7*, 11515. [CrossRef]

117. Schütz, C.; Van Rie, J.; Eyley, S.; Gençer, A.; Van Gorp, H.; Rosenfeldt, S.; Kang, K.; Thielemans, W. Effect of Source on the Properties and Behavior of Cellulose Nanocrystal Suspensions. *ACS Sustain. Chem. Eng.* **2018**, *6*, 8317–8324. [CrossRef]

118. Zhu, B.; Johansen, V.E.; Kamita, G.; Guidetti, G.; Bay, M.M.; Parton, T.G.; Frka-Petesic, B.; Vignolini, S. Hyperspectral Imaging of Photonic Cellulose Nanocrystal Films: Structure of Local Defects and Implications for Self-Assembly Pathways. *ACS Nano* **2020**, *14*, 15361–15373. [CrossRef]

119. Peppas, N.A.; Hilt, J.Z.; Khademhosseini, A.; Langer, R. Hydrogels in Biology and Medicine: From Molecular Principles to Bionanotechnology. *Adv. Mater.* **2006**, *18*, 1345–1360. [CrossRef]

120. Slaughter, B.V.; Khurshid, S.S.; Fisher, O.Z.; Khademhosseini, A.; Peppas, N.A. Hydrogels in Regenerative Medicine. *Adv. Mater.* **2009**, *21*, 3307–3329. [CrossRef] [PubMed]

121. Kobayashi, H.; Ikada, Y.; Moritera, T.; Ogura, Y.; Honda, Y. Collagen-Immobilized Hydrogel as a Material for Lamellar Keratoplasty. *J. Appl. Biomater. Off. J. Soc. Biomater.* **1991**, *2*, 261–267. [CrossRef] [PubMed]

122. Freed, L.E.; Marquis, J.C.; Nohria, A.; Emmanual, J.; Mikos, A.G.; Langer, R. Neocartilage Formation in Vitro and in Vivo Using Cells Cultured on Synthetic Biodegradable Polymers. *J. Biomed. Mater. Res.* **1993**, *27*, 11–23. [CrossRef]

123. Sui, Z.; King, W.J.; Murphy, W.L. Protein-Based Hydrogels with Tunable Dynamic Responses. *Adv. Funct. Mater.* **2008**, *18*, 1824–1831. [CrossRef]

124. Tang, Z.; Wang, Y.; Podsiadlo, P.; Kotov, N.A. Biomedical Applications of Layer-by-Layer Assembly: From Biomimetics to Tissue Engineering. *Adv. Mater.* **2006**, *18*, 3203–3224. [CrossRef]

125. McGuigan, A.P.; Sefton, M.V. Vascularized Organoid Engineered by Modular Assembly Enables Blood Perfusion. *Proc. Natl. Acad. Sci. USA* **2006**, *103*, 11461–11466. [CrossRef]

126. Nerem, R.M. Cellular Engineering. *Ann. Biomed. Eng.* **1991**, *19*, 529–545. [CrossRef]

127. Langer, R. New Methods of Drug Delivery. *Science* **1990**, *249*, 1527–1533. [CrossRef]

128. Buschmann, M.D.; Gluzband, Y.A.; Grodzinsky, A.J.; Kimura, J.H.; Hunziker, E.B. Chondrocytes in Agarose Culture Synthesize a Mechanically Functional Extracellular Matrix. *J. Orthop. Res.* **1992**, *10*, 745–758. [CrossRef] [PubMed]

129. Sawhney, A.S.; Hubbell, J.A. Poly(Ethylene Oxide)-Graft-Poly(L-Lysine) Copolymers to Enhance the Biocompatibility of Poly(L-Lysine)-Alginate Microcapsule Membranes. *Biomaterials* **1992**, *13*, 863–870. [CrossRef]

130. Langer, R.; Vacanti, J.P. Tissue Engineering. *Science* **1993**, *260*, 920–926. [CrossRef]

131. Langer, R.; Peppas, N.A. Advances in Biomaterials, Drug Delivery, and Bionanotechnology. *AIChE J.* **2003**, *49*, 2990–3006. [CrossRef]

132. Franzesi, G.T.; Ni, B.; Ling, Y.; Khademhosseini, A. A Controlled-Release Strategy for the Generation of Cross-Linked Hydrogel Microstructures. *J. Am. Chem. Soc.* **2006**, *128*, 15064–15065. [CrossRef] [PubMed]

133. Cabodi, M.; Choi, N.W.; Gleghorn, J.P.; Lee, C.S.D.; Bonassar, L.J.; Strook, A.D. A Microfluidic Biomaterial. *J. Am. Chem. Soc.* **2005**, *127*, 13788–13789. [CrossRef]

134. Balog, E.R.M.; Ghosh, K.; Park, Y.I.; Hartung, V.; Sista, P.; Rocha, R.C.; Wang, H.L.; Martinez, J.S. Stimuli-Responsive Genetically Engineered Polymer Hydrogel Demonstrates Emergent Optical Responses. *ACS Biomater. Sci. Eng.* **2016**, *2*, 1135–1142. [CrossRef]

135. Wang, E.; Desai, M.S.; Lee, S.W. Light-Controlled Graphene-Elastin Composite Hydrogel Actuators. *Nano Lett.* **2013**, *13*, 2826–2830. [CrossRef] [PubMed]

136. Gulrez, S.K.; Al-Assaf, S.; Phillips, G.O. Hydrogels: Methods of Preparation, Characterisation and Applications. In *Progress in Molecular and Environmental Bioengineering—From Analysis and Modeling to Technology Applications*; InTech: London, UK, 2011.

137. Alonso, M.; Reboto, V.; Guiscardo, L.; San Martín, A.; Rodríguez-Cabello, J.C. Spiropyran Derivative of an Elastin-like Bioelastic Polymer: Photoresponsive Molecular Machine to Convert Sunlight into Mechanical Work. *Macromolecules* **2000**, *33*, 9480–9482. [CrossRef]

138. Annabi, N.; Mithieux, S.M.; Weiss, A.S.; Dehghani, F. The Fabrication of Elastin-Based Hydrogels Using High Pressure CO2. *Biomaterials* **2009**, *30*, 1–7. [CrossRef]

139. Sun, Z.; Qin, G.; Xia, X.; Cronin-Golomb, M.; Omenetto, F.G.; Kaplan, D.L. Photoresponsive Retinal-Modified Silk-Elastin Copolymer. *J. Am. Chem. Soc.* **2013**, *135*, 3675–3679. [CrossRef] [PubMed]

140. Sun, Y.L.; Dong, W.F.; Niu, L.G.; Jiang, T.; Liu, D.X.; Zhang, L.; Wang, Y.S.; Chen, Q.D.; Kim, D.P.; Sun, H.B. Protein-Based Soft Micro-Optics Fabricated by Femtosecond Laser Direct Writing. *Light Sci. Appl.* **2014**, *3*, e129. [CrossRef]

141. Dong, L.; Agarwal, A.K.; Beebe, D.J.; Jiang, H. Adaptive Liquid Microlenses Activated by Stimuli-Responsive Hydrogels. *Nature* **2006**, *442*, 551–554. [CrossRef] [PubMed]

142. Melikov, R.; Press, D.A.; Kumar, B.G.; Dogru, I.B.; Sadeghi, S.; Chirea, M.; Yilgör, I.; Nizamoglu, S. Silk-Hydrogel Lenses for Light-Emitting Diodes. *Sci. Rep.* **2017**, *7*, 7258. [CrossRef]

143. Mayer, M.; Yang, J.; Gitlin, I.; Gracias, D.H.; Whitesides, G.M. Micropatterned Agarose Gels for Stamping Arrays of Proteins and Gradients of Proteins. *GM Proteom.* **2004**, *4*, 2366. [CrossRef]

144. Jain, A.; Yang, A.H.J.; Erickson, D. Gel-Based Optical Waveguides with Live Cell Encapsulation and Integrated Microfluidics. *Opt. Lett.* **2012**, *37*, 1472. [CrossRef]

145. Fujiwara, E.; Cabral, T.D.; Sato, M.; Oku, H.; Cordeiro, C.M.B. Agarose-Based Structured Optical Fibre. *Sci. Rep.* **2020**, *10*, 7035. [CrossRef]

146. Gao, R.; Jiang, Y.; Ding, W. Agarose Gel Filled Temperature-Insensitive Photonic Crystal Fibers Humidity Sensor Based on the Tunable Coupling Ratio. *Sens. Actuators B Chem.* **2014**, *195*, 313–319. [CrossRef]

147. Gambino, S.; Mazzeo, M.; Genco, A.; Di Stefano, O.; Savasta, S.; Patanè, S.; Ballarini, D.; Mangione, F.; Lerario, G.; Sanvitto, D.; et al. Exploring Light-Matter Interaction Phenomena under Ultrastrong Coupling Regime. *ACS Photonics* **2014**, *1*, 1042–1048. [CrossRef]

148. Abdi-Jalebi, M.; Andaji-Garmaroudi, Z.; Cacovich, S.; Stavrakas, C.; Philippe, B.; Richter, J.M.; Alsari, M.; Booker, E.P.; Hutter, E.M.; Pearson, A.J.; et al. Maximizing and Stabilizing Luminescence from Halide Perovskites with Potassium Passivation. *Nature* **2018**, *555*, 497–501. [CrossRef]

149. Akkerman, Q.A.; Rainò, G.; Kovalenko, M.V.; Manna, L. Genesis, Challenges and Opportunities for Colloidal Lead Halide Perovskite Nanocrystals. *Nat. Mater.* **2018**, *17*, 394–405. [CrossRef]

150. Akkerman, Q.A.; D'Innocenzo, V.; Accornero, S.; Scarpellini, A.; Petrozza, A.; Prato, M.; Manna, L. Tuning the Optical Properties of Cesium Lead Halide Perovskite Nanocrystals by Anion Exchange Reactions. *J. Am. Chem. Soc.* **2015**, *137*, 10276–10281. [CrossRef]

151. Burda, C.; Chen, X.; Narayanan, R.; El-Sayed, M.A. Chemistry and Properties of Nanocrystals of Different Shapes. *Chem. Rev.* **2005**, *105*, 1025–1102. [CrossRef]

152. Press, D.; De Greve, K.; McMahon, P.L.; Ladd, T.D.; Friess, B.; Schneider, C.; Kamp, M.; Höfling, S.; Forchel, A.; Yamamoto, Y. Ultrafast Optical Spin Echo in a Single Quantum Dot. *Nat. Photonics* **2010**, *4*, 367–370. [CrossRef]

153. Lund-Hansen, T.; Stobbe, S.; Julsgaard, B.; Thyrrestrup, H.; Sünner, T.; Kamp, M.; Forchel, A.; Lodahl, P. Experimental Realization of Highly Efficient Broadband Coupling of Single Quantum Dots to a Photonic Crystal Waveguide. *Phys. Rev. Lett.* **2008**, *101*, 113903. [CrossRef] [PubMed]

154. Klenovský, P.; Schliwa, A.; Bimberg, D. Electronic States of (InGa)(AsSb)/GaAs/GaP Quantum Dots. *Phys. Rev. B* **2019**, *100*, 115424. [CrossRef]

155. Grundmann, M.; Stier, O.; Bimberg, D. InAs/GaAs Pyramidal Quantum Dots: Strain Distribution, Optical Phonons, and Electronic Structure. *Phys. Rev. B* **1995**, *52*, 11969–11981. [CrossRef]

156. Michalet, X.; Pinaud, F.F.; Bentolila, L.A.; Tsay, J.M.; Doose, S.; Li, J.J.; Sundaresan, G.; Wu, A.M.; Gambhir, S.S.; Weiss, S. Quantum Dots for Live Cells, in Vivo Imaging, and Diagnostics. *Science* **2005**, *307*, 538–544. [CrossRef] [PubMed]

157. Alivisatos, A.P. Semiconductor Clusters, Nanocrystals, and Quantum Dots. *Science* **1996**, *271*, 933–937. [CrossRef]

158. Palei, M.; Caligiuri, V.; Kudera, S.; Krahne, R. Robust and Bright Photoluminescence from Colloidal Nanocrystal/Al2O3 Composite Films Fabricated by Atomic Layer Deposition. *ACS Appl. Mater. Interfaces* **2018**, *10*, 22356–22362. [CrossRef]

159. Castelli, A.; Dhanabalan, B.; Polovitsyn, A.; Caligiuri, V.; Di Stasio, F.; Scarpellini, A.; Brescia, R.; Palei, M.; Martín-García, B.; Prato, M.; et al. Core/Shell CdSe/CdS Bone-Shaped Nanocrystals with a Thick and Anisotropic Shell as Optical Emitters. *Adv. Opt. Mater.* **2019**, *8*, 1901463. [CrossRef]

160. Verlick, S.F. Fluorescence Spectra and Polarization of Glyceraldehyde-3-Phosphate and Lactic Dehydrogenase Coenzyme Complexes. *J. Biol. Chem.* **1958**, *233*, 1455–1467. [CrossRef]

161. Schaefer, P.M.; Kalinina, S.; Rueck, A.; von Arnim, C.A.F.; von Einem, B. NADH Autofluorescence—A Marker on Its Way to Boost Bioenergetic Research. *Cytom. Part A* **2019**, *95*, 34–46. [CrossRef] [PubMed]

162. You, S.; Tu, H.; Chaney, E.J.; Sun, Y.; Zhao, Y.; Bower, A.J.; Liu, Y.Z.; Marjanovic, M.; Sinha, S.; Pu, Y.; et al. Intravital Imaging by Simultaneous Label-Free Autofluorescence-Multiharmonic Microscopy. *Nat. Commun.* **2018**, *9*, 2125. [CrossRef] [PubMed]

163. Blacker, T.S.; Mann, Z.F.; Gale, J.E.; Ziegler, M.; Bain, A.J.; Szabadkai, G.; Duchen, M.R. Separating NADH and NADPH Fluorescence in Live Cells and Tissues Using FLIM. *Nat. Commun.* **2014**, *5*, 3936. [CrossRef]

164. Rocheleau, J.V.; Head, W.S.; Piston, D.W. Quantitative NAD(P)H/Flavoprotein Autofluorescence Imaging Reveals Metabolic Mechanisms of Pancreatic Islet Pyruvate Response. *J. Biol. Chem.* **2004**, *279*, 31780–31787. [CrossRef]

165. Ying, W. NAD+/NADH and NADP+/NADPH in Cellular Functions and Cell Death: Regulation and Biological Consequences. *Antioxid. Redox Signal.* **2008**, *10*, 179–206. [CrossRef] [PubMed]

166. Kolenc, O.I.; Quinn, K.P. Evaluating Cell Metabolism through Autofluorescence Imaging of NAD(P)H and FAD. *Antioxid. Redox Signal.* **2019**, *30*, 875–889. [CrossRef]

167. Alam, S.R.; Wallrabe, H.; Svindrych, Z.; Chaudhary, A.K.; Christopher, K.G.; Chandra, D.; Periasamy, A. Investigation of Mitochondrial Metabolic Response to Doxorubicin in Prostate Cancer Cells: An NADH, FAD and Tryptophan FLIM Assay. *Sci. Rep.* **2017**, *7*, 10451. [CrossRef]

168. Liu, Z.; Pouli, D.; Alonzo, C.A.; Varone, A.; Karaliota, S.; Quinn, K.P.; Mönger, K.; Karalis, K.P.; Georgakoudi, I. Mapping Metabolic Changes by Noninvasive, Multiparametric, High-Resolution Imaging Using Endogenous Contrast. *Sci. Adv.* **2018**, *4*, eaap9302. [CrossRef]

169. Churchich, J.E. Fluorescence Properties of Pyridoxamine 5-Phosphate. *BBA Biophys. Incl. Photosynth.* **1965**, *102*, 280–288. [CrossRef]

170. Hughes, C.F.; Ward, M.; Tracey, F.; Hoey, L.; Molloy, A.M.; Pentieva, K.; McNulty, H. B-Vitamin Intake and Biomarker Status in Relation to Cognitive Decline in Healthy Older Adults in a 4-Year Follow-up Study. *Nutrients* **2017**, *9*, 53. [CrossRef] [PubMed]
171. Pilicer, S.L.; Bakhshi, P.R.; Bentley, K.W.; Wolf, C. Biomimetic Chirality Sensing with Pyridoxal-5′-Phosphate. *J. Am. Chem. Soc.* **2017**, *139*, 1758–1761. [CrossRef] [PubMed]
172. Upadhyay, Y.; Anand, T.; Babu, L.T.; Paira, P.; Crisponi, G.; Sk, A.K.; Kumar, R.; Sahoo, S.K. Three-in-One Type Fluorescent Sensor Based on a Pyrene Pyridoxal Cascade for the Selective Detection of Zn(II), Hydrogen Phosphate and Cysteine. *Dalton Trans.* **2018**, *47*, 742–749. [CrossRef]
173. Halawa, M.I.; Gao, W.; Saqib, M.; Kitte, S.A.; Wu, F.; Xu, G. Sensitive Detection of Alkaline Phosphatase by Switching on Gold Nanoclusters Fluorescence Quenched by Pyridoxal Phosphate. *Biosens. Bioelectron.* **2017**, *95*, 8–14. [CrossRef]
174. Passannante, A.J.; Avioli, L.V. Studies on the Ultraviolet Fluorescence of Vitamin D and Related Compounds in Acid-Alcohol Solutions. *Anal. Biochem.* **1966**, *15*, 287–295. [CrossRef]
175. Zähringer, K. The Use of Vitamins as Tracer Dyes for Laser-Induced Fluorescence in Liquid Flow Applications. *Exp. Fluids* **2014**, *55*, 1712. [CrossRef]
176. Rubin, M. Fluorometry and Phosphorimetry in Clinical Chemistry. *Adv. Clin. Chem.* **1970**, *13*, 161–269. [CrossRef]
177. Xue, X.; Hu, L.; Hou, Z. *Study on Fluorescence Spectra of B Vitamins*; Atlantis Press: Amsterdam, The Netherlands, 2016; pp. 85–90.
178. Zhang, Y.; Yang, J. Design Strategies for Fluorescent Biodegradable Polymeric Biomaterials. *J. Mater. Chem. B* **2013**, *1*, 132–148. [CrossRef]
179. Rodrigues, A.C.B.; de Melo, J.S.S. Aggregation-Induced Emission: From Small Molecules to Polymers—Historical Background, Mechanisms and Photophysics. *Top. Curr. Chem.* **2021**, *379*, 15. [CrossRef] [PubMed]
180. Cai, X.; Liu, B. Aggregation-Induced Emission: Recent Advances in Materials and Biomedical Applications. *Angew. Chem. Int. Ed.* **2020**, *59*, 9868–9886. [CrossRef] [PubMed]
181. Zhu, C.; Kwok, R.T.K.; Lam, J.W.Y.; Tang, B.Z. Aggregation-Induced Emission: A Trailblazing Journey to the Field of Biomedicine. *ACS Appl. Bio Mater.* **2018**, *1*, 1768–1786. [CrossRef]
182. Xi, Y.; Gao, W.; Chen, J.; Zhang, S.; Yang, T.; Gao, B. Biocompatible Fluorescent Probe with the Aggregation-Induced Emission Characteristic for Live Cell Imaging. In Proceedings of the International Symposium on Materials Application and Engineering (SMAE 2016), Chiang Mai, Thailand, 20 August 2016. [CrossRef]
183. Xu, D.; Liu, M.; Zou, H.; Tian, J.; Huang, H.; Wan, Q.; Dai, Y.; Wen, Y.; Zhang, X.; Wei, Y. A New Strategy for Fabrication of Water Dispersible and Biodegradable Fluorescent Organic Nanoparticles with AIE and ESIPT Characteristics and Their Utilization for Bioimaging. *Talanta* **2017**, *174*, 803–808. [CrossRef] [PubMed]
184. Luo, J.; Xie, Z.; Xie, Z.; Lam, J.W.Y.; Cheng, L.; Chen, H.; Qiu, C.; Kwok, H.S.; Zhan, X.; Liu, Y.; et al. Aggregation-Induced Emission of 1-Methyl-1,2,3,4,5-Pentaphenylsilole. *Chem. Commun.* **2001**, *18*, 1740–1741. [CrossRef]
185. Wu, Y.T.; Kuo, M.Y.; Chang, Y.T.; Shin, C.C.; Wu, T.C.; Tai, C.C.; Cheng, T.H.; Liu, W.S. Synthesis, Structure, and Photophysical Properties of Highly Substituted 8,8a-Dihydrocyclopenta[a]Indenes. *Angew. Chem. Int. Ed.* **2008**, *47*, 9891–9894. [CrossRef]
186. Shimizu, M.; Takeda, Y.; Higashi, M.; Hiyama, T. 1,4-Bis(Alkenyl)-2,5-Dipiperidinobenzenes: Minimal Fluorophores Exhibiting Highly Efficient Emission in the Solid State. *Angew. Chem. Int. Ed.* **2009**, *48*, 3653–3656. [CrossRef] [PubMed]
187. An, B.K.; Kwon, S.K.; Jung, S.D.; Park, S.Y. Enhanced Emission and Its Switching in Fluorescent Organic Nanoparticles. *J. Am. Chem. Soc.* **2002**, *124*, 14410–14415. [CrossRef] [PubMed]
188. Birkedal, H.; Pattison, P. Bis[4-(Salicylideneamino)Phenyl]-Methane. *Acta Crystallogr. Sect. C Cryst. Struct. Commun.* **2006**, *62*, o139–o141. [CrossRef]
189. Mutai, T.; Tomoda, H.; Ohkawa, T.; Yabe, Y.; Araki, K. Switching of Polymorph-Dependent ESIPT Luminescence of an Imidazo[1,2-a]Pyridine Derivative. *Angew. Chem. Int. Ed.* **2008**, *47*, 9522–9524. [CrossRef] [PubMed]
190. Zhou, T.; Li, F.; Fan, Y.; Song, W.; Mu, X.; Zhang, H.; Wang, Y. Hydrogen-Bonded Dimer Stacking Induced Emission of Aminobenzoic Acid Compounds. *Chem. Commun.* **2009**, 3199–3201. [CrossRef]
191. Liu, J.; Lam, J.W.Y.; Tang, B.Z. Acetylenic Polymers: Syntheses, Structures, and Functions. *Chem. Rev.* **2009**, *109*, 5799–5867. [CrossRef]
192. Liu, Y.; Feng, X.; Shi, J.B.; Zhi, J.G.; Tong, B.; Dong, Y.P. Aggregation-Induced Emission Enhancement in Poly(Phenyleneethynylene)s Bearing Aniline Groups. *Chin. J. Polym. Sci.* **2012**, *30*, 443–450. [CrossRef]
193. Pucci, A.; Rausa, R.; Ciardelli, F. Aggregation-Induced Luminescence of Polyisobutene Succinic Anhydrides and Imides. *Macromol. Chem. Phys.* **2008**, *209*, 900–906. [CrossRef]
194. Ruff, Y.; Lehn, J.M. Glycodynamers: Fluorescent Dynamic Analogues of Polysaccharides. *Angew. Chem. Int. Ed.* **2008**, *47*, 3556–3559. [CrossRef] [PubMed]
195. Ruff, Y.; Buhler, E.; Candau, S.J.; Kesselman, E.; Talmon, Y.; Lehn, J.M. Glycodynamers: Dynamic Polymers Bearing Oligosaccharides Residues - Generation, Structure, Physicochemical, Component Exchange, and Lectin Binding Properties. *J. Am. Chem. Soc.* **2010**, *132*, 2573–2584. [CrossRef] [PubMed]
196. Liu, J.; Lam, J.W.Y.; Tang, B.Z. Aggregation-Induced Emission of Silole Molecules and Polymers: Fundamental and Applications. *J. Inorg. Organomet. Polym. Mater.* **2009**, *19*, 249–285. [CrossRef]
197. Hong, Y.; Lam, J.W.Y.; Tang, B.Z. Aggregation-Induced Emission. *Chem. Soc. Rev* **2011**, *40*, 5361–5388. [CrossRef]
198. Dong, J.; Solntsevn, K.M.; Tolbert, L.M. Activation and Tuning of Green Fluorescent Protein Chromophore Emission by Alkyl Substituent-Mediated Crystal Packing. *J. Am. Chem. Soc.* **2009**, *131*, 662–670. [CrossRef]

199. Debler, E.W.; Kaufmann, G.F.; Meijler, M.M.; Heine, A.; Mee, J.M.; Pljevaljčić, G.; Di Bilio, A.J.; Schultz, P.G.; Millar, D.P.; Janda, K.D.; et al. Deeply Inverted Electron-Hole Recombination in a Luminescent Antibody-Stilbene Complex. *Science* **2008**, *319*, 1232–1235. [CrossRef] [PubMed]

200. Tian, F.; Debler, E.W.; Millar, D.P.; Deniz, A.A.; Wilson, I.A.; Schultz, P.G. The Effects of Antibodies on Stilbene Excited-State Energetics. *Angew. Chem. Int. Ed.* **2006**, *45*, 7763–7765. [CrossRef]

201. Glazer, A.N. Light Harvesting by Phycobilisomes. *Annu. Rev. Biophys. Biophys. Chem.* **1985**, *14*, 47–77. [CrossRef]

202. Lakowicz, J.R. *Principles of Fluorescence Spectroscopy*; Springer US: New York, NY, USA, 2006; ISBN 978-0-387-31278-1.

203. Glazer, A.N. Phycobiliproteins—a Family of Valuable, Widely Used Fluorophores. *J. Appl. Phycol.* **1994**, *6*, 105–112. [CrossRef]

204. Gantt, E. Structure and Function of Phycobilisomes: Light-Harvesting Pigment Complexes in Red and Blue-Green Algae. *Int. Rev. Cytol.* **1980**, *56*, 45–80.

205. DeLange, R.J.; Glazer, A.G. Phycoerythrin Fluorescence-Based Assay for Peroxy Radicals: A Screen for Biologically Relevant Protective Agents. *Anal. Biochem.* **1989**, *177*, 300–306. [CrossRef]

206. Grabowski, J.; Gantt, E. Photophysical Properties of Phycobiliproteins from Phycobilisomes: Fluorescence Lifetimes, Quantum Yields, and Polarization Spectra. *Photochem. Photobiol.* **1978**, *28*, 39–45. [CrossRef]

207. Cohen-Bazire, G.; Beguin, S.; Rimon, S.; Glazer, A.N.; Brown, D.M. Physico-Chemical and Immunological Properties of Allophycocyanins. *Arch. Microbiol.* **1977**, *111*, 225–238. [CrossRef]

208. Glazer, A.N.; Stryer, L. Phycofluor Probes. *Trends Biochem. Sci.* **1984**, *9*, 423–427. [CrossRef]

209. Rüdiger, W.; Thümmler, F. The phytochrome chromophore. In *Photomorphogenesis in Plants*; Springer: Dordrecht, The Netherlands, 1994; pp. 51–69.

210. Murphy, J.T.; Lagarias, J.C. The Phytofluors: A New Class of Fluorescent Protein Probes. *Curr. Biol.* **1997**, *7*, 870–876. [CrossRef]

211. Fischer, A.J.; Lagarias, J.C. Harnessing Phytochrome's Glowing Potential. *Proc. Natl. Acad. Sci. USA* **2004**, *101*, 17334–17339. [CrossRef] [PubMed]

212. Gambetta, G.A.; Lagarias, J.C. Genetic Engineering of Phytochrome Biosynthesis in Bacteria. *Proc. Natl. Acad. Sci. USA* **2001**, *98*, 10566–10571. [CrossRef] [PubMed]

213. Chalfie, M.; Tu, Y.; Euskirchen, G.; Ward, W.W.; Prasher, D.C. Green Fluorescent Protein as a Marker for Gene Expression. *Science* **1994**, *263*, 802–805. [CrossRef] [PubMed]

214. Cody, C.W.; Prasher, D.C.; Westler, W.M.; Prendergast, F.G.; Ward, W.W. Chemical Structure of the Hexapeptide Chromophore of the Aequorea Green-Fluorescent Protein. *Biochemistry* **1993**, *32*, 1212–1218. [CrossRef] [PubMed]

215. Reid, B.G.; Flynn, G.C. Chromophore Formation in Green Fluorescent Protein. *Biochemistry* **1997**, *36*, 6786–6791. [CrossRef]

216. Shimomura, O.; Johnson, F.H.; Saiga, Y. Extraction, Purification and Properties of Aequorin, a Bioluminescent. *J. Cell. Comp. Physiol.* **1962**, *59*, 223–239. [CrossRef]

217. Shimomura, O. A Short Story of Aequorin. *Biol. Bull.* **1995**, *189*, 1–5. [CrossRef]

218. Remington, S.J. Green Fluorescent Protein: A Perspective. *Protein Sci.* **2011**, *20*, 1509–1519. [CrossRef]

219. Barondeau, D.P.; Putnam, C.D.; Kassmann, C.J.; Tainer, J.A.; Getzoff, E.D. Mechanism and Energetics of Green Fluorescent Protein Chromophore Synthesis Revealed by Trapped Intermediate Structures. *Proc. Natl. Acad. Sci. USA* **2003**, *100*, 12111–12116. [CrossRef]

220. Shi, S.; Kumar, P.; Lee, K.F. Generation of Photonic Entanglement in Green Fluorescent Proteins. *Nat. Commun.* **2017**, *8*, 1934. [CrossRef]

221. Yuan, Z.; Zhou, Y.; Qiao, Z.; Eng Aik, C.; Tu, W.C.; Wu, X.; Chen, Y.C. Stimulated Chiral Light-Matter Interactions in Biological Microlasers. *ACS Nano* **2021**, *15*, 8975. [CrossRef]

222. Karl, M.; Meek, A.; Murawski, C.; Tropf, L.; Keum, C.; Schubert, M.; Samuel, I.D.W.; Turnbull, G.A.; Gather, M.C. Distributed Feedback Lasers Based on Green Fluorescent Protein and Conformal High Refractive Index Oxide Layers. *Laser Photonics Rev.* **2020**, *14*, 2000101. [CrossRef]

223. Dogru, I.B.; Min, K.; Umar, M.; Bahmani Jalali, H.; Begar, E.; Conkar, D.; Firat Karalar, E.N.; Kim, S.; Nizamoglu, S. Single Transverse Mode Protein Laser. *Appl. Phys. Lett.* **2017**, *111*, 231103. [CrossRef]

224. Oh, H.J.; Gather, M.C.; Song, J.-J.; Yun, S.H. Lasing from Fluorescent Protein Crystals. *Opt. Express* **2014**, *22*, 31411. [CrossRef]

225. Gather, M.C.; Yun, S.H. Single-Cell Biological Lasers. *Nat. Photonics* **2011**, *5*, 406–410. [CrossRef]

226. Gather, M.C.; Yun, S.H. Lasing from Escherichia Coli Bacteria Genetically Programmed to Express Green Fluorescent Protein. *Opt. Lett.* **2011**, *36*, 3299–3301. [CrossRef]

227. Weber, M.D.; Niklaus, L.; Pröschel, M.; Coto, P.B.; Sonnewald, U.; Costa, R.D. Bioinspired Hybrid White Light-Emitting Diodes. *Adv. Mater.* **2015**, *27*, 5493–5498. [CrossRef] [PubMed]

228. Bajar, B.T.; Wang, E.S.; Zhang, S.; Lin, M.Z.; Chu, J. A Guide to Fluorescent Protein FRET Pairs. *Sensors* **2016**, *16*, 1488. [CrossRef] [PubMed]

229. Zajac, J.M.; Schubert, M.; Roland, T.; Keum, C.; Samuel, I.D.W.; Gather, M.C. Time-Resolved Studies of Energy Transfer in Thin Films of Green and Red Fluorescent Proteins. *Adv. Funct. Mater.* **2018**, *28*, 1706300. [CrossRef]

230. Lelimousin, M.; Noirclerc-Savoye, M.; Lazareno-Saez, C.; Paetzold, B.; Le Vot, S.; Chazal, R.; Macheboeuf, P.; Field, M.J.; Bourgeois, D.; Royant, A. Intrinsic Dynamics in ECFP and Cerulean Control Fluorescence Quantum Yield. *Biochemistry* **2009**, *48*, 10038–10046. [CrossRef]

231. Goedhart, J.; Van Weeren, L.; Hink, M.A.; Vischer, N.O.E.; Jalink, K.; Gadella, T.W.J. Bright Cyan Fluorescent Protein Variants Identified by Fluorescence Lifetime Screening. *Nat. Methods* **2010**, *7*, 137–139. [CrossRef]

232. Rizzo, M.A.; Springer, G.H.; Granada, B.; Piston, D.W. An Improved Cyan Fluorescent Protein Variant Useful for FRET. *Nat. Biotechnol.* **2004**, *22*, 445–449. [CrossRef] [PubMed]

233. Goedhart, J.; Von Stetten, D.; Noirclerc-Savoye, M.; Lelimousin, M.; Joosen, L.; Hink, M.A.; Van Weeren, L.; Gadella, T.W.J.; Royant, A. Structure-Guided Evolution of Cyan Fluorescent Proteins towards a Quantum Yield of 93%. *Nat. Commun.* **2012**, *3*, 751. [CrossRef] [PubMed]

234. Erard, M.; Fredj, A.; Pasquier, H.; Beltolngar, D.B.; Bousmah, Y.; Derrien, V.; Vincent, P.; Merola, F. Minimum Set of Mutations Needed to Optimize Cyan Fluorescent Proteins for Live Cell Imaging. *Mol. Biosyst.* **2013**, *9*, 258–267. [CrossRef] [PubMed]

235. Villoing, A.; Ridhoir, M.; Cinquin, B.; Erard, M.; Alvarez, L.; Vallverdu, G.; Pernot, P.; Grailhe, R.; Mérola, F.; Pasquier, H. Complex Fluorescence of the Cyan Fluorescent Protein: Comparisons with the H148D Variant and Consequences for Quantitative Cell Imaging. *Biochemistry* **2008**, *47*, 12483–12492. [CrossRef]

236. Tramier, M.; Zahid, M.; Mevel, J.C.; Masse, M.J.; Coppey-Moisan, M. Sensitivity of CFP/YFP and GFP/MCherry Pairs to Donor Photobleaching on FRET Determination by Fluorescence Lifetime Imaging Microscopy in Living Cells. *Microsc. Res. Tech.* **2006**, *69*, 933–939. [CrossRef]

237. Espagne, A.; Erard, M.; Madiona, K.; Derrien, V.; Jonasson, G.; Lévy, B.; Pasquier, H.; Melki, R.; Mèrola, F. Cyan Fluorescent Protein Carries a Constitutive Mutation That Prevents Its Dimerization. *Biochemistry* **2011**, *50*, 437–439. [CrossRef]

238. Markwardt, M.L.; Kremers, G.J.; Kraft, C.A.; Ray, K.; Cranfill, P.J.C.; Wilson, K.A.; Day, R.N.; Wachter, R.M.; Davidson, M.W.; Rizzo, M.A. An Improved Cerulean Fluorescent Protein with Enhanced Brightness and Reduced Reversible Photoswitching. *PLoS ONE* **2011**, *6*, 17896. [CrossRef]

239. Kremers, G.J.; Goedhart, J.; Van Munster, E.B.; Gadella, T.W.J. Cyan and Yellow Super Fluorescent Proteins with Improved Brightness, Protein Folding, and FRET Förster Radius. *Biochemistry* **2006**, *45*, 6570–6580. [CrossRef]

240. Pletneva, N.V.; Pletnev, V.Z.; Souslova, E.; Chudakov, D.M.; Lukyanov, S.; Martynov, V.I.; Arhipova, S.; Artemyev, I.; Wlodawer, A.; Dauter, Z.; et al. Yellow Fluorescent Protein PhiYFPv (Phialidium): Structure and Structure-Based Mutagenesis. *Acta Crystallogr. Sect. D Biol. Crystallogr.* **2013**, *69*, 1005–1012. [CrossRef]

241. Nagai, T.; Ibata, K.; Park, E.S.; Kubota, M.; Mikoshiba, K.; Miyawaki, A. A Variant of Yellow Fluorescent Protein with Fast and Efficient Maturation for Cell-Biological Applications. *Nat. Biotechnol.* **2002**, *20*, 87–90. [CrossRef]

242. Rekas, A.; Alattia, J.R.; Nagai, T.; Miyawaki, A.; Ikura, M. Crystal Structure of Venus, a Yellow Fluorescent Protein with Improved Maturation and Reduced Environmental Sensitivity. *J. Biol. Chem.* **2002**, *277*, 50573–50578. [CrossRef] [PubMed]

243. Kredel, S.; Oswald, F.; Nienhaus, K.; Deuschle, K.; Röcker, C.; Wolff, M.; Heilker, R.; Nienhaus, G.U.; Wiedenmann, J. MRuby, a Bright Monomeric Red Fluorescent Protein for Labeling of Subcellular Structures. *PLoS ONE* **2009**, *4*, 4391. [CrossRef] [PubMed]

244. Hense, A.; Nienhaus, K.; Nienhaus, G.U. Exploring Color Tuning Strategies in Red Fluorescent Proteins. *Photochem. Photobiol. Sci.* **2015**, *14*, 200–212. [CrossRef] [PubMed]

245. Dedecker, P.; De Schryver, F.C.; Hofkens, J. Fluorescent Proteins: Shine on, You Crazy Diamond. *J. Am. Chem. Soc.* **2013**, *135*, 2387–2402. [CrossRef] [PubMed]

246. Kredel, S.; Nienhaus, K.; Oswald, F.; Wolff, M.; Ivanchenko, S.; Cymer, F.; Jeromin, A.; Michel, F.J.; Spindler, K.D.; Heilker, R.; et al. Optimized and Far-Red-Emitting Variants of Fluorescent Protein EqFP611. *Chem. Biol.* **2008**, *15*, 224–233. [CrossRef]

247. Hense, A.; Prunsche, B.; Gao, P.; Ishitsuka, Y.; Nienhaus, K.; Nienhaus, G.U. Monomeric Garnet, a Far-Red Fluorescent Protein for Live-Cell STED Imaging. *Sci. Rep.* **2015**, *5*, 18006. [CrossRef] [PubMed]

248. Shcherbo, D.; Murphy, C.S.; Ermakova, G.V.; Solovieva, E.A.; Chepurnykh, T.V.; Shcheglov, A.S.; Verkhusha, V.V.; Pletnev, V.Z.; Hazelwood, K.L.; Roche, P.M.; et al. Far-Red Fluorescent Tags for Protein Imaging in Living Tissues. *Biochem. J.* **2009**, *418*, 567–574. [CrossRef]

249. Chung, P.-H.; Tregidgo, C.; Suhling, K. Determining a Fluorophore's Transition Dipole Moment from Fluorescence Lifetime Measurements in Solvents of Varying Refractive Index. *Methods Appl. Fluoresc.* **2016**, *4*, 045001. [CrossRef]

250. Uudsemaa, M.; Trummal, A.; de Reguardati, S.; Callis, P.R.; Rebane, A. TD-DFT Calculations of One- and Two-Photon Absorption in Coumarin C153 and Prodan: Attuning Theory to Experiment. *Phys. Chem. Chem. Phys.* **2017**, *19*, 28824–28833. [CrossRef]

251. Pandey, N.; Gahlaut, R.; Arora, P.; Joshi, N.K.; Joshi, H.C.; Pant, S. Study of Dipole Moments of Some Coumarin Derivatives. *J. Mol. Struct.* **2014**, *1061*, 175–180. [CrossRef]

252. Nifosì, R.; Mennucci, B.; Filippi, C. The Key to the Yellow-to-Cyan Tuning in the Green Fluorescent Protein Family Is Polarisation. *Phys. Chem. Chem. Phys.* **2019**, *21*, 18988–18998. [CrossRef] [PubMed]